Initiation of the Southern Elsinore Fault at ∼1.2 Ma: Evidence from the Fish Creek–Vallecito Basin, southern California

Rebecca J. Dorsey,[1] Gary J. Axen,[2] Thomas C. Peryam,[1] and Mary E. Kairouz[3,4]

Received 18 August 2011; revised 11 January 2012; accepted 19 January 2012; published 16 March 2012.

[1] Strike-slip faults west of the San Andreas fault (SAF) accommodate more than half of the modern Pacific–North America plate motion in southern California, yet their age, kinematic evolution and long-term slip rates are incompletely understood. The southern Elsinore fault is part of this zone and occupies the boundary between Mesozoic crystalline rocks of the Peninsular Ranges and Late Cenozoic sedimentary rocks of the Salton Trough depocenter. The Fish Creek–Vallecito Basin, a recently inverted western sub-basin of the Salton Trough, contains a thick succession of Plio-Pleistocene sedimentary rocks that preserve a record of crustal subsidence and uplift in response to evolving tectonic controls. Deposits older than ∼1.2 Ma accumulated during transtension and subsidence in the hanging wall of the low-angle West Salton detachment fault. A fanning-dip interval high in the section, dated at 1.2–1.0 Ma, accumulated during tilting caused by earliest motion on the Elsinore and Earthquake Valley faults. Total offset of 1–2 km yields a lifetime slip rate of about 1–2 mm/yr for the southern Elsinore fault, similar to a late Pleistocene rate in the Coyote Mountains but slower than published estimates for the northern Elsinore fault. This difference likely results from long-term transfer of slip from the northern Elsinore fault to the San Felipe and San Jacinto fault zones farther east. Initiation of the Elsinore fault at 1.2 Ma coincides with a major tectonic reorganization that terminated slip on the detachment fault and formed the modern network of strike-slip faults west of the SAF.

Citation: Dorsey, R. J., G. J. Axen, T. C. Peryam, and M. E. Kairouz (2012), Initiation of the Southern Elsinore Fault at ∼1.2 Ma: Evidence from the Fish Creek–Vallecito Basin, southern California, *Tectonics*, *31*, TC2006, doi:10.1029/2011TC003009.

1. Introduction

[2] The San Andreas fault system in southern California (Figure 1) is an ∼80-km wide zone of dextral deformation that accommodates relative motion between the Pacific and North America plates [e.g., *Humphreys and Weldon*, 1994; *Bennett et al.*, 1996; *Meade and Hager*, 2005]. The time-space partitioning of strain in the San Andreas system is important for understanding fault dynamics, seismic hazards, and geodynamic controls on crustal deformation. Active faults west of the San Andreas, including the San Jacinto, San Felipe, and Elsinore faults, accommodate more than half of the total plate motion in southern California [e.g., *Fialko*, 2006; *Janecke et al.*, 2010], yet their age, kinematic evolution and long-term slip rates remain uncertain and debated. Some studies extrapolate late Pleistocene slip rates back in time to infer that the San Jacinto fault initiated ca. 1.8–2.5 Ma [e.g., *Rockwell et al.*, 1990; *Blisniuk et al.*, 2010], while others conclude from geologic data that the San Jacinto and San Felipe faults initiated around 1.1–1.4 Ma [*Morton and Matti*, 1993; *Lutz et al.*, 2006; *Kirby et al.*, 2007; *Steely et al.*, 2009; *Janecke et al.*, 2010]. Contrasting ages have also been proposed for the Elsinore and Earthquake Valley faults, as summarized below, creating uncertainty about fault zone evolution and long-term slip rates.

[3] The Fish Creek–Vallecito Basin (Figure 2) contains a thick succession of Late Cenozoic sedimentary rocks [*Winker*, 1987; *Winker and Kidwell*, 1996; *Dorsey et al.*, 2011] that provide useful constraints on the age of strike-slip fault initiation at the western margin of the Salton Trough. *Johnson et al.* [1983] concluded that the end of deposition and change to uplift was caused by initiation of the Elsinore fault at ∼1.0 Ma. In contrast, *Magistrale and Rockwell* [1996] proposed that prior to 1 Ma, the Fish Creek–Vallecito Basin formed as a pull-apart basin in a releasing stepover between the San Felipe fault in the north and the Coyote Mountains strand of the Elsinore fault in the south (Figure 2). They inferred that the onset of uplift and erosion resulted from *reorganization*, not initiation, of the

[1]Department of Geological Sciences, University of Oregon, Eugene, Oregon, USA.
[2]Department of Earth and Environmental Science, New Mexico Institute of Mining and Technology, Socorro, New Mexico, USA.
[3]Department of Earth and Space Science, University of California, Los Angeles, California, USA.
[4]Now at AMEC Environment and Infrastructure, Socorro, New Mexico, USA.

0278-7407/12/2011TC003009

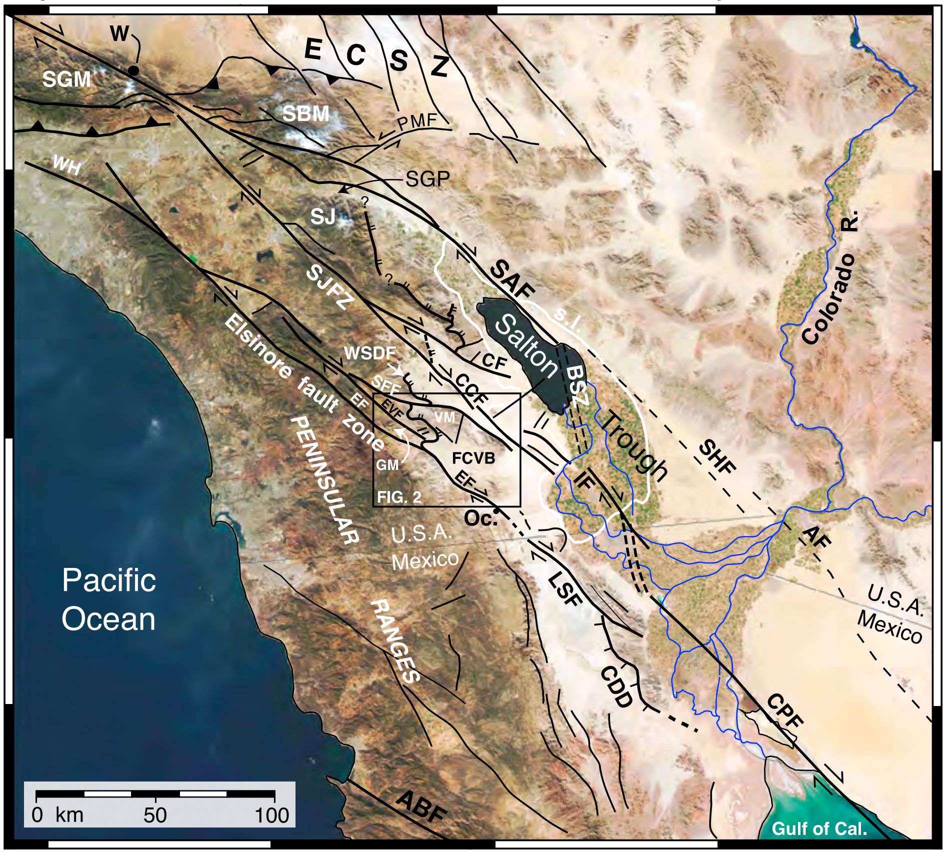

Figure 1. Map of major faults in southern California and northwest Mexico. The southern San Andreas fault system includes the San Andreas, San Jacinto, San Felipe, and Elsinore fault zones. ABF, Agua Blanca fault; AF, Algodones fault; BSZ, Brawley seismic zone; CCF, Coyote Creek fault; CDD, Canada David detachment; CF, Clark fault; CPF, Cerro Prieto fault; ECSZ, Eastern California shear zone; EF, Elsinore fault; EVF, Earthquake Valley fault; FCVB, Fish Creek–Vallecito Basin; GM, Granite Mountain; IF, Imperial fault; LSF, Laguna Salada fault; Oc., town of Ocotillo; PMF, Pinto Mountain fault; SAF, San Andreas fault; SBM, San Bernardino Mtns; SHF, Sand Hills fault; SFF, San Felipe fault; SGM, San Gabriel Mountains; SGP, San Gorgonio Pass; SJ, San Jacinto peak; SJFZ, San Jacinto fault zone; VM, Vallecito Mountains; W, Wrightwood; WH, Whittier Hills; WSDF, West Salton detachment fault. White line labeled "s.l" is sea level.

Elsinore fault zone. More recent studies have shown that subsidence prior to ∼1 Ma took place in a supradetachment basin that was bounded on the west by the West Salton detachment fault [*Axen and Fletcher*, 1998; *Kairouz*, 2005; *Axen*, 2008], prior to initiation of the currently active system of strike-slip faults. These contrasting interpretations for the Fish Creek–Vallecito Basin highlight uncertainties about the timing and tectonic controls on crustal subsidence, post-depositional inversion, and the age and significance of the Elsinore and Earthquake Valley faults.

[4] This paper describes a study of Pleistocene strata in the Fish Creek–Vallecito Basin and the transition from subsidence and deposition to the modern phase of uplift (inversion), erosion and dextral-wrench deformation. We present the results of detailed geologic mapping, stratigraphic and structural analysis, combined with existing age constraints, to reconstruct the timing, style, and surface response to initiation of modern strike-slip faults. In particular, we address the following questions: (1) when did subsidence and slip on the basin-bounding West Salton detachment fault end; (2) what was the role of the Elsinore and Earthquake Valley faults in the change to basin uplift and inversion; (3) how did the landscape respond to the structural transition from detachment to strike-slip faulting; and (4) what is the stratigraphic record of these processes? We find that slip on the detachment fault ended at the same time as initiation of the Elsinore and related strike-slip faults at ∼1.0–1.2 Ma, during a major tectonic reorganization of the southern San Andreas fault system. This study thus highlights the importance of integrated mapping, stratigraphic and structural analysis for understanding complex structural transitions in tectonically active settings.

2. Geologic Setting

[5] The West Salton detachment fault is a regional, low-angle, normal to oblique-normal fault that was active from late Miocene or early Pliocene time [*Axen and Fletcher*, 1998; *Shirvell et al.*, 2009] to ca. 1.1–1.3 Ma [*Steely et al.*, 2009]. Total horizontal extension on the detachment fault

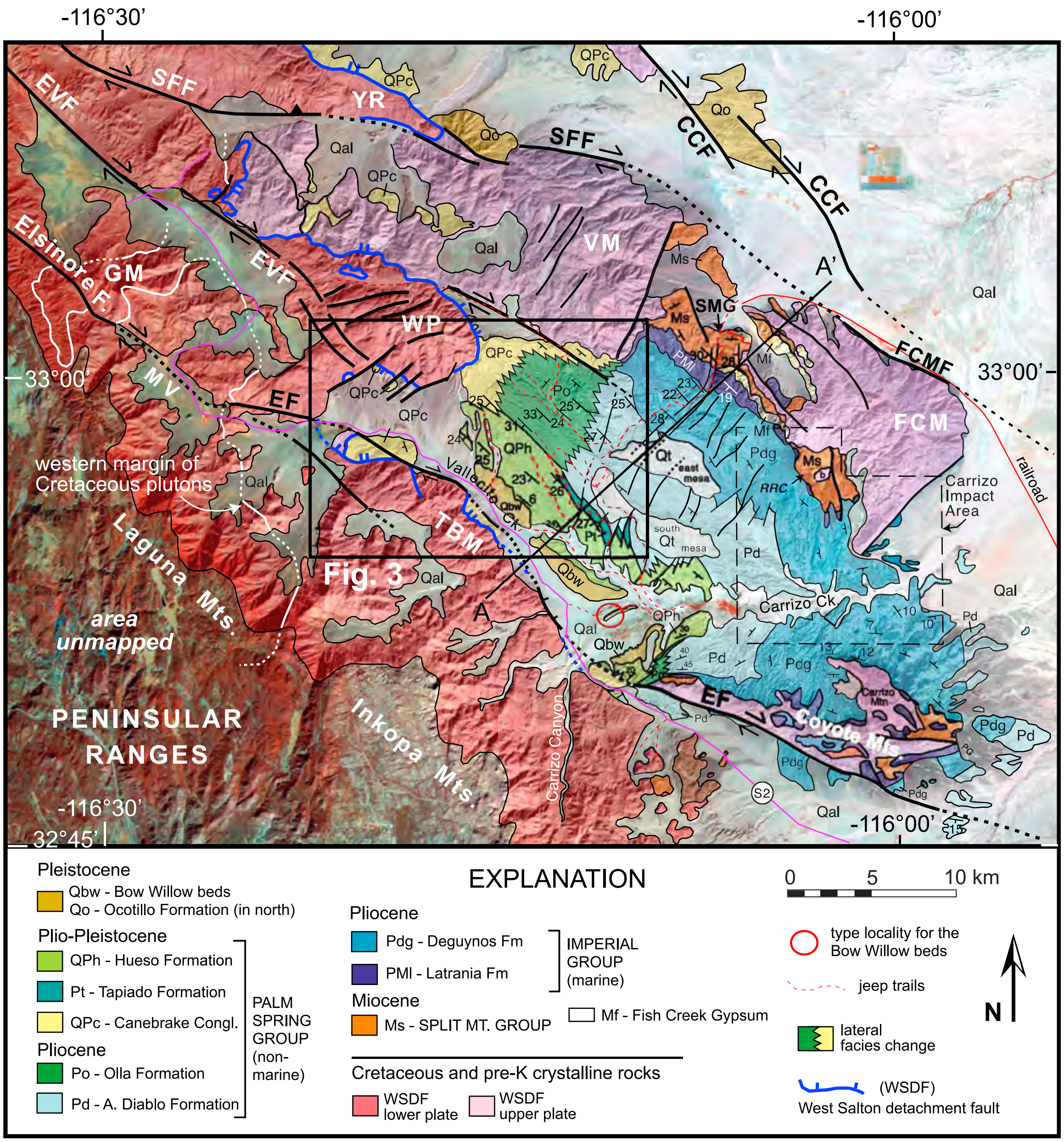

Figure 2. Simplified geologic map of the Fish Creek–Vallecito Basin and surrounding area, modified from *Winker* [1987], *Winker and Kidwell* [1996], *Dibblee* [1996], *Axen and Fletcher* [1998], *Grove et al.* [2003], *Kairouz* [2005], and *Steely et al.* [2009]. CCF, Coyote Creek fault; FCM, Fish Creek Mountains; FCMF, Fish Creek Mountains fault; GM, Granite Mountain; MV, Mason Valley; RRC, Red Rock Canyon; SFF, San Felipe fault; SMG, Split Mt. Gorge; TBM, Tierra Blanca Mountains; VM, Vallecito Mountains; YR, Yaqui Ridge; WP, Whale Peak. Line A-A′ is line of restored geologic cross section in Figure 12.

is estimated from thermobarometry to be about 8–10 km [*Shirvell et al.*, 2009]. Pliocene to early Pleistocene deposition in the Fish Creek–Vallecito Basin took place as a result of subsidence in the hanging wall of the West Salton detachment fault [*Axen and Fletcher*, 1998; *Kairouz*, 2005; *Axen*, 2008; this study]. The early Pleistocene Canebrake Conglomerate is cut by the detachment fault on the south flank of Whale Peak, indicating that slip on the detachment continued until ca. 1 Ma (Figures 3 and 4) [*Kairouz*, 2005]. Since about 1 Ma the detachment fault has been structurally dismembered and offset by younger strike-slip faults, including strands of the Elsinore and Earthquake Valley faults and related smaller faults. The details, timing, and style of this structural transition were, until this study, poorly understood.

[6] The Elsinore fault zone trends obliquely across the Peninsular Ranges from the Whittier Hills in the northwest to the town of Ocotillo in the southeast, connecting to the Laguna Salada fault in northern Mexico (Figure 1). Total offset in the northwest is estimated at 10–15 km based on

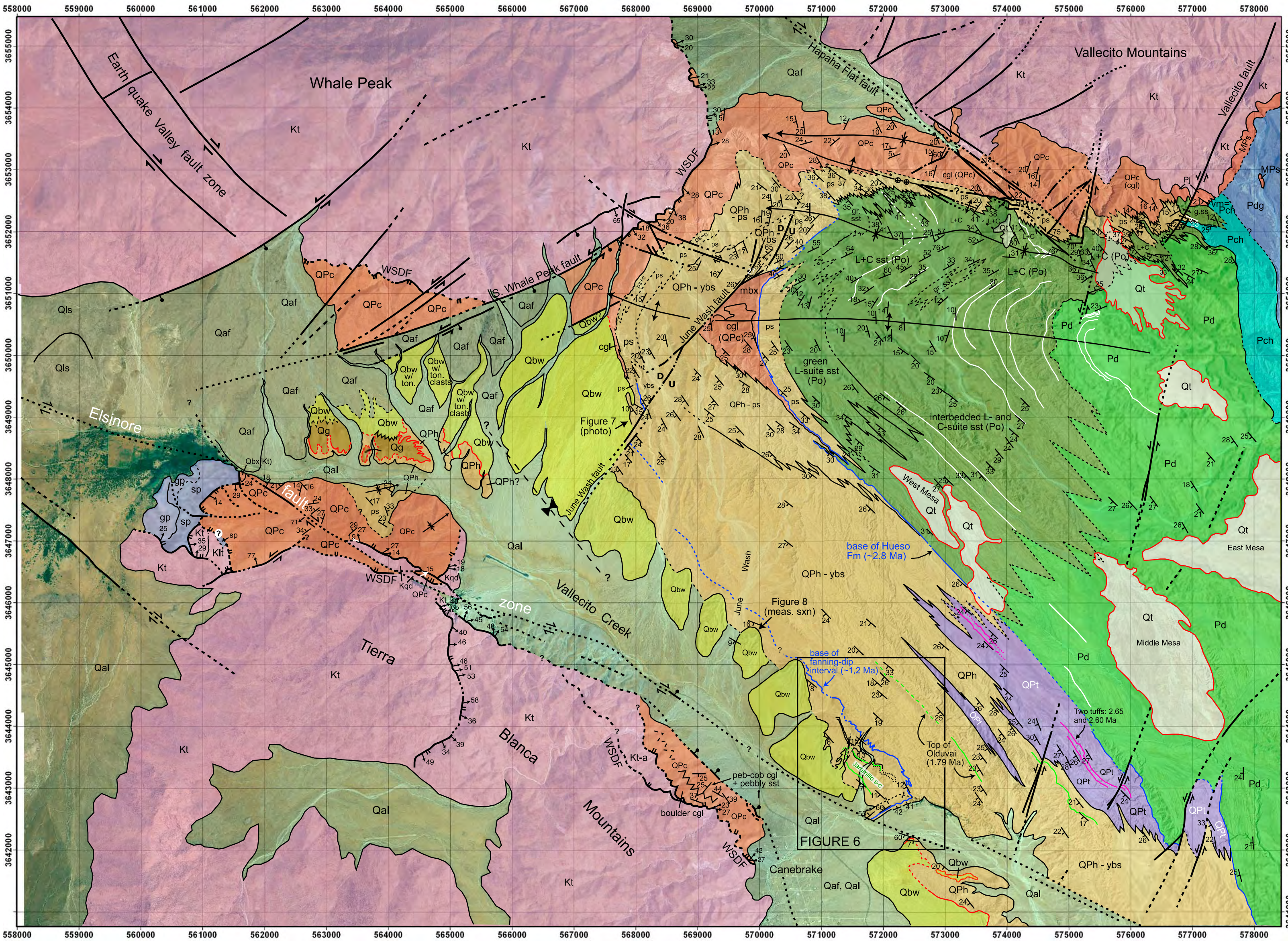

Figure 3. Geologic map of the northwestern Fish Creek–Vallecito Basin, based on detailed 1:10,000- and 1:20,000-scale mapping carried out for this study. White lines internal to map units indicate bedding form lines and marker beds. Blue lines mark base of Hueso formation and base of fanning-dip interval. Red lines indicate unconformities. Pink lines are ash beds in the Tapiado Formation.

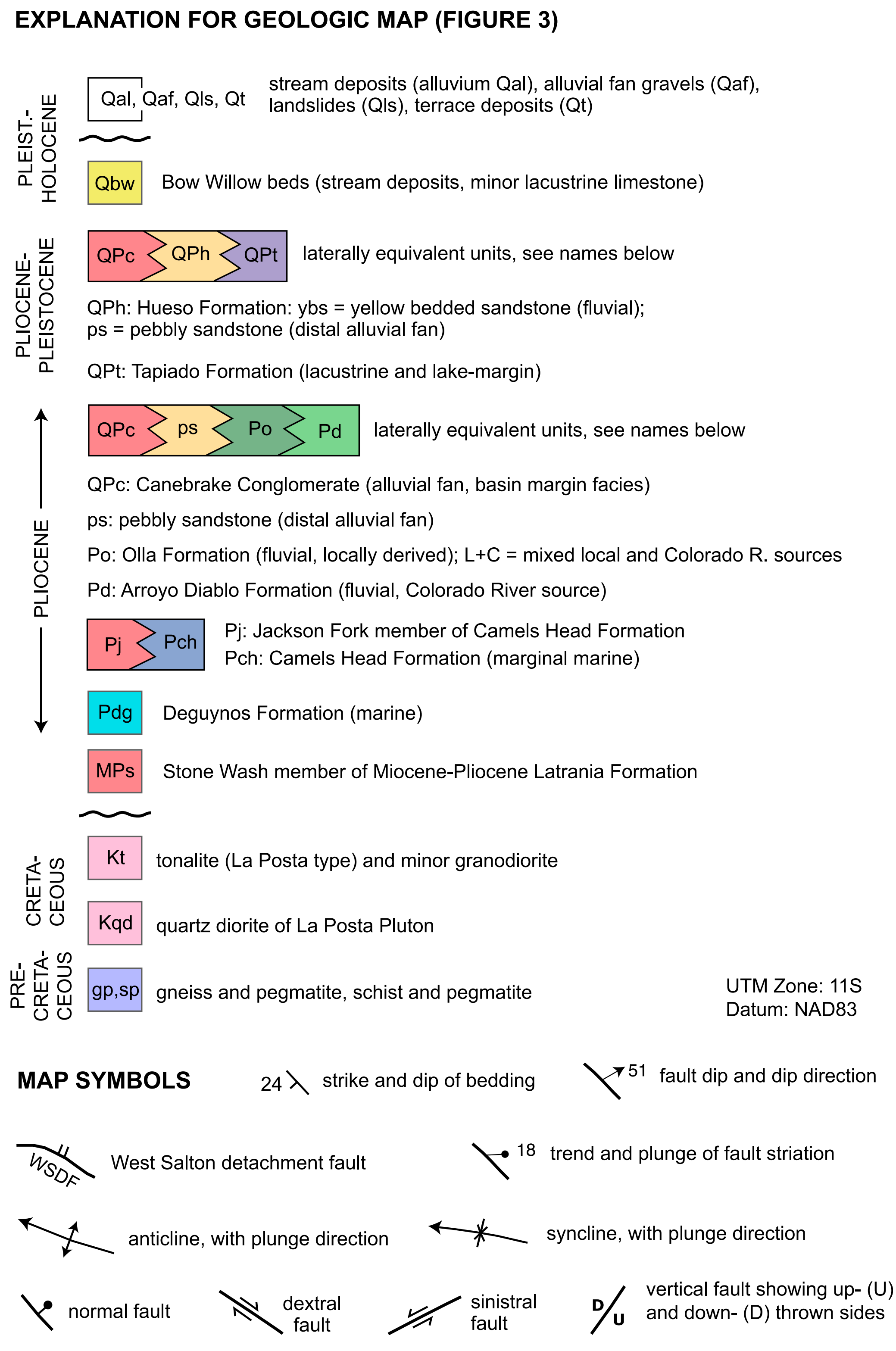

Figure 3. (continued)

correlation of crystalline rocks [*Weber*, 1977; *Morton and Miller*, 1987] and a late Miocene basalt field [*Hull*, 1990; *Hull and Nicholson*, 1992]. Assuming that the 2.5-Ma Temecula Arkose was controlled by early faulting, the long-term slip rate is inferred to be about 4–6 mm/yr in the north [*Hull and Nicholson*, 1992]. This is generally consistent with late Pleistocene to Holocene rates of 3–6 mm/yr (prior studies summarized by *Magistrale and Rockwell* [1996]), including a Holocene rate of 3.3–5.5 mm/yr on the southern Elsinore fault in the Coyote Mountains [*Pinault and*

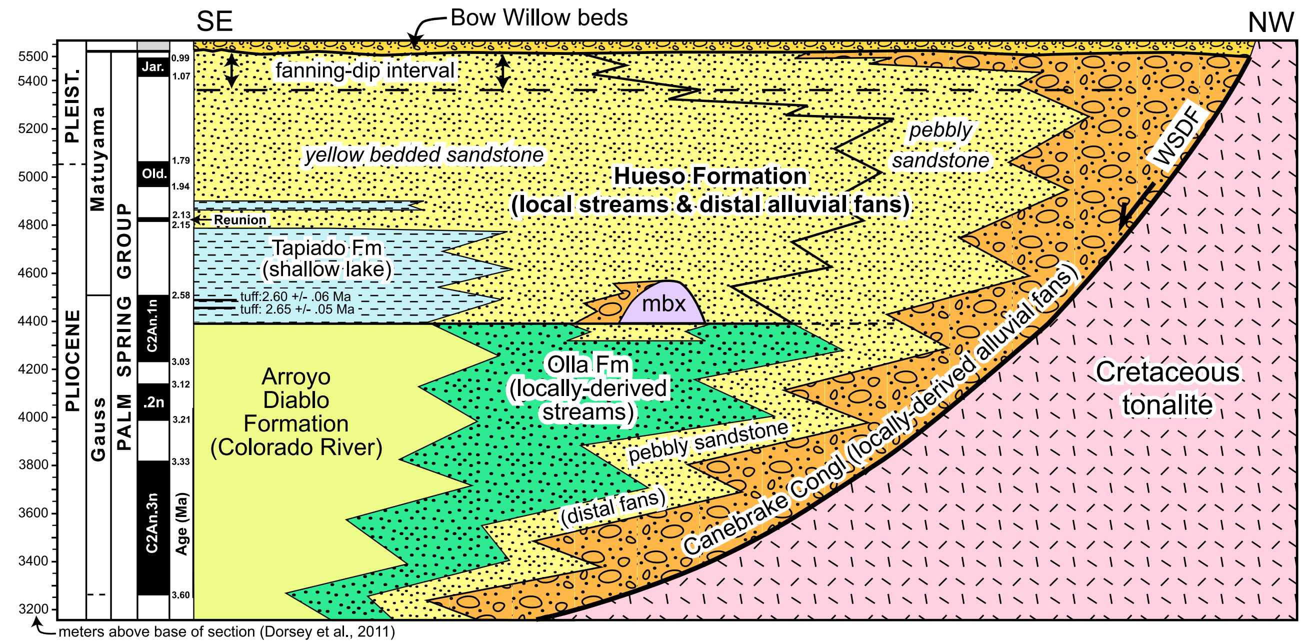

Figure 4. Simplified NW-SE facies panel for the northwestern Fish Creek–Vallecito Basin. Thicknesses, magnetostratigraphy, and ages of tuffs from *Dorsey et al.* [2011]. Lateral facies relationships based on geologic mapping (this study). MBX represents tonalitic megabreccia derived from Whale Peak. Listric form of WSDF is speculative.

Rockwell, 1984]. A slower rate of 1.6 ± 0.4 mm/yr over the past ~40 kyr was recently determined from U-series dating of soil carbonate in offset alluvial fans in the Coyote Mountains [*Fletcher et al.*, 2011], though the authors of that study suggested the slip rate may increase sharply along strike to the northwest. Geodetic data indicate that the Elsinore fault presently is accumulating negligible interseismic strain despite abundant microseismicity [*Fialko*, 2006].

[7] Total bedrock offset on the Elsinore fault decreases southward from 10 to 15 km in the northwest to ~2 km at Granite Mountain and 1 km at the southeast end of Mason Valley (Figure 2) [*Lampe*, 1988; *Grove et al.*, 2003]. This discrepancy has led some workers to suggest that the remaining ~7.5–12.5 km of offset is transferred NE to the Earthquake Valley fault [*Magistrale and Rockwell*, 1996]. However, limited offset on the Earthquake Valley fault near Whale Peak [*Kairouz*, 2005] suggests that much of the offset on the northern Elsinore fault zone may instead be transferred east to the San Felipe fault, which has ~6 ± 3 km of dextral offset and feeds slip east and southeast to the Fish Creek Mountains and Coyote Creek faults [*Steely et al.*, 2009].

[8] The northwestern Fish Creek–Vallecito Basin is a structurally complex setting where Plio-Pleistocene sedimentary rocks are in depositional and fault contact with Cretaceous and older crystalline rocks of the eastern Peninsular Ranges (Figures 2 and 3). Magnetostratigraphic studies show that the basin-filling section ranges in age from ~8 Ma at the base to 0.9–1.0 Ma at the top [*Opdyke et al.*, 1977; *Johnson et al.*, 1983; *Dorsey et al.*, 2007, 2011]. The upper ~2,300 m of section includes fluvial and lacustrine deposits of the Hueso and Tapiado formations and laterally equivalent basin-margin facies of the Canebrake Conglomerate that range in age from about 3.6 to 1.0 Ma (Figure 4). The deposits dip to the southwest, with notable variations around folds and adjacent to large faults, so the youngest sediments in the section are located just northeast of Vallecito Creek near the faulted southwestern margin of the basin (Figures 2 and 3).

[9] Crystalline bedrock surrounding the Fish Creek–Vallecito Basin consists mainly of granitic plutonic rocks of the Cretaceous Peninsular Ranges batholith (primarily tonalite of the mid-Cretaceous La Posta pluton), intruded into Paleozoic to early Mesozoic metasedimentary and Early Cretaceous metavolcanic rocks [e.g., *Todd et al.*, 2003; *Grove et al.*, 2003; and citations therein]. Around the basin, these rocks lie in the footwall of the West Salton detachment fault (Figure 2) and form the primary source terrain for locally derived sedimentary rocks in the basin.

3. Stratigraphy

[10] Sedimentary rocks in the western Fish Creek–Vallecito Basin are subdivided here into three stratigraphic intervals (Figure 4): (1) Plio-Pleistocene units that accumulated during slip on the West Salton detachment fault; (2) fanning-dip interval, bracketed between ~1.2 and 1.0 Ma, that records earliest intrabasinal tilting related to initiation of strike-slip faults; and (3) post-1.0 Ma deposits that post-date the detachment fault and accumulated during slip on the modern system of strike-slip faults. The age of the deposits is well known from prior magnetostratigraphic studies in which magnetic reversals were correlated to the geomagnetic polarity time scale using two dated tuffs just below the 2.58-Ma Gauss-Matuyama boundary (Figure 4) [*Opdyke et al.*, 1977; *Johnson et al.*, 1983; *Dorsey et al.*, 2011].

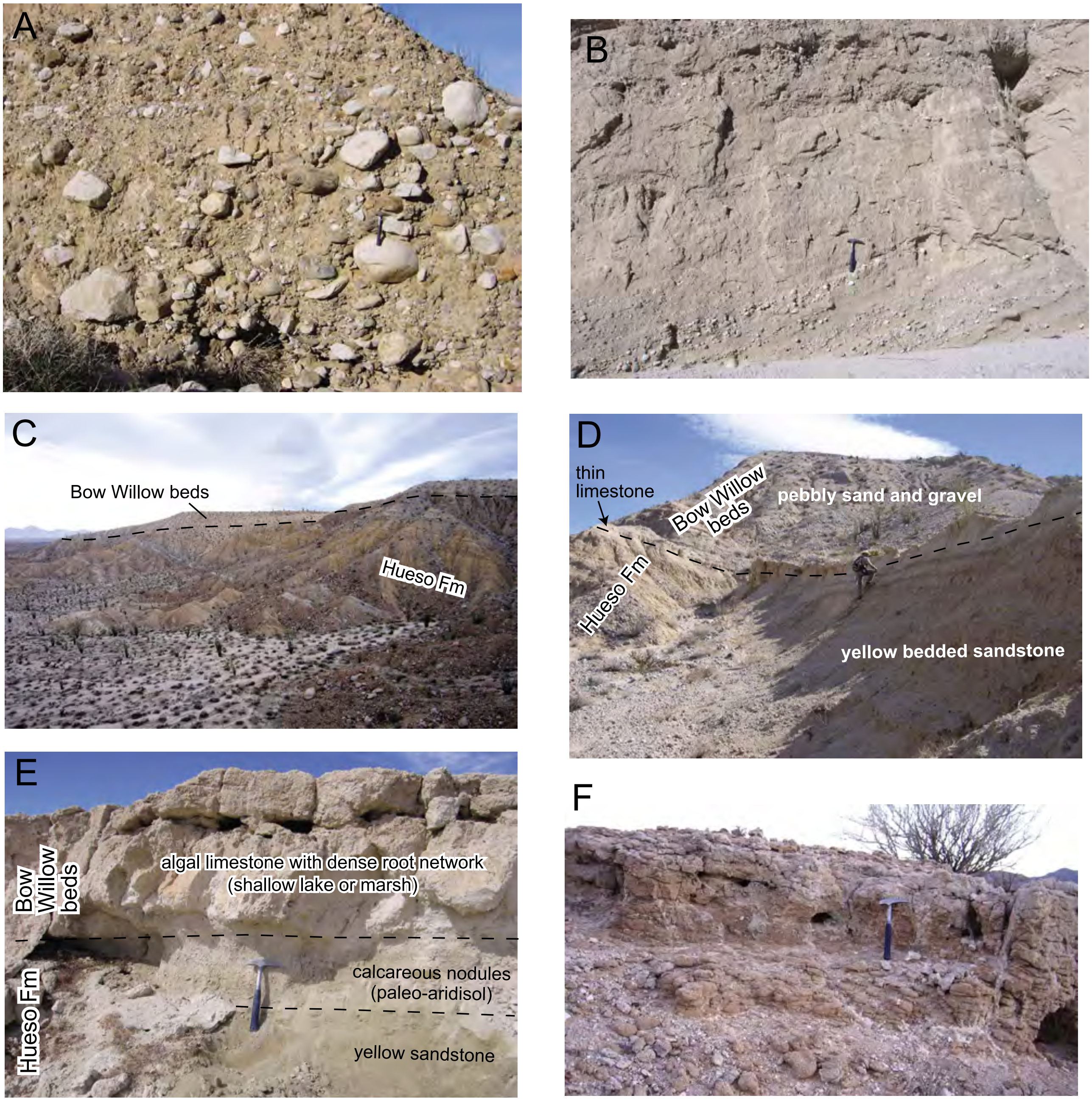

Figure 5. Photographs of sedimentary rocks exposed in the northwestern Fish Creek–Vallecito Basin. (a) Canebrake Conglomerate, consisting of poorly sorted debris-flow facies that record deposition in proximal alluvial fans. (b) Typical example of pebbly sandstone in the Hueso Formation, deposited in distal alluvial fans and ephemeral streams. (c) Hueso Formation overlain by Bow Willow beds along an angular unconformity (dashed line). (d) Uppermost Hueso Formation (top of fanning-dip interval) conformably overlain by Bow Willow beds in lower June Wash (Figure 3). (e) Close-up photo of contact between Hueso Formation and basal Bow Willow beds (shallow-lacustrine limestone), see Figure 6 for location. (f) Deep calcite-filled fissures in thick calcic paleosol which caps and truncates the top of the Bow Willow beds.

3.1. Plio-Pleistocene Units

[11] Plio-Pleistocene units in the study area (through the Hueso Formation) belong to the Palm Spring Group (Figures 3 and 4) [*Winker and Kidwell*, 1996; *Cassiliano*, 1999]. The lower part of the Palm Spring Group includes quartz-rich sandstone and red mudstone of the Arroyo Diablo Formation that accumulated in fluvio-deltaic channels and overbank environments of the lower Colorado River, and laterally equivalent Canebrake Conglomerate (Figure 5a; locally derived alluvial fans) and Olla Formation sandstone (mixed-composition streams). A narrow belt of pebbly sandstone in the lateral transition between the Canebrake and Olla formations records deposition in distal

alluvial fans. The overall transgressive architecture of these deposits records translation of the upper plate of the West Salton detachment fault eastward away from the lower-plate source of locally derived sediment during sedimentation.

[12] An abrupt change in stratigraphic architecture at ~4,400 m records reorganization of the basin at ca. 2.8 Ma (Figure 4) [*Winker*, 1987; *Dorsey et al.*, 2011]. Above this datum the upper Palm Spring Group includes locally sourced fluvial sandstone and pebbly sandstone of the Hueso Formation (Figure 5b), which interfingers with laterally equivalent Tapiado Formation (lacustrine mudstone and siltstone) and Canebrake Conglomerate (alluvial fans). This stratigraphic boundary is marked by a monolithologic megabreccia composed of Cretaceous tonalite likely derived from Whale Peak to the north (Figures 3 and 4). The megabreccia is overlain by a fining-upward unit of Canebrake Conglomerate that contains clasts of both Cretaceous tonalite and pre-Cretaceous metamorphic rocks exposed west of the basin (Figure 2). The upper part of the Palm Spring Group close to Whale Peak displays a coarsening-up trend that records progradation of gravelly alluvial fans (Canebrake Conglomerate) to the south or southeast over finer-grained sandy fluvial deposits (Hueso Formation) (Figure 4).

3.2. Fanning-Dip Interval

[13] The upper ~100–200 m of the Hueso Formation is an interval of sandstone, pebbly sandstone and minor conglomerate that displays distinctive wedge-like geometries in map pattern (Figures 3 and 6) and systematic up-section decrease in bedding dip (Figure 7). The age of this interval is determined from detailed geologic mapping in lower View of the Badlands Wash (Figure 6), combined with magnetostratigraphic data of *Dorsey et al.* [2011]. The base of the fanning-dip interval is about 250 m map distance stratigraphically below the base of the Jaramillo subchron, which at an average dip of ~12° represents a stratigraphic thickness of ~52 m. The age of this horizon (base of the fanning-dip interval) is estimated from linear interpolation to be about 1.2 Ma. It is difficult to assign an exact uncertainty to this value, but the steadiness of accumulation rate in this part of the section [*Dorsey et al.*, 2011] lends confidence to the linear interpolation and suggests an uncertainty of around 5–10% (+/−~0.1 Ma) in the age of the base of the fanning-dip interval. The top of the fanning-dip interval is the base of the very gently dipping Bow Willow beds, ~10–30 m above the top of the Jaramillo subchron (0.99 Ma). The upper part of the fanning-dip interval north of the June Wash fault passes laterally north toward Whale Peak into the youngest part of the Canebrake Conglomerate (Figures 3 and 4), indicating that footwall-derived conglomerate as young as ca. 1.0 Ma is cut by the low-angle West Salton detachment fault.

3.3. Post–1 Ma Units

[14] Sediments younger than ~1 Ma include the Bow Willow beds and all younger deposits of Quaternary alluvium, colluvium, terraces, landslides and alluvial fans (Figures 3 and 4). "Bow Willow beds" (previously Mesa Conglomerate) is an informal local name that is applied here to resolve problems with existing nomenclature. The Mesa Conglomerate, defined by *Woodard* [1963] and mapped by *Todd* [2004], includes both flat-lying Quaternary gravels that cap large mesas in the study area and gently dipping deposits of gravel, sand, siltstone, and minor limestone (Bow Willow beds, this study) that are exposed along Bow Willow, Vallecito, and Carrizo creeks. The type example of the Mesa Conglomerate was identified by *Woodard* [1963] as flat-lying terrace gravels exposed on the eroded south edge of West Mesa, but new observations show that the mesa-capping gravels are significantly younger than the gently dipping deposits, and thus the two units have a different stratigraphic position and should not be mapped as the same formation. Moreover, the common name "Mesa" is nonunique and may be confused with other units with the same name elsewhere [e.g., *Mencher et al.*, 1953; *Dorsey and Burns*, 1994; *Cox et al.*, 2006]. We therefore divide deposits previously assigned to the Mesa Conglomerate into two map units (Figure 3): (1) late Quaternary flat lying terrace gravels (Qt) that cap large mesas in the study area; and (2) the older Bow Willow beds (Qbw), defined here as gently dipping Quaternary deposits that overlie the Hueso Formation within ~2–4 km of the detachment fault. The type locality for the Bow Willow beds is in lower Bow Willow Creek (UTM coordinates: zone 11S; 576,550 E; 3,637,350 N; NAD 83) where it is well exposed in low cliffs south of the wash (Figure 2).

[15] The Bow Willow beds consist of weakly cemented sandstone, sandy conglomerate and pebbly sandstone that generally coarsen toward range fronts, with thickness varying between about 5 and 30 m (Figure 8). Away from range fronts the deposits include fine to coarse grained sandstone, siltstone, and minor mudstone with variably developed calcic paleosols. The Bow Willow beds overlie the Hueso Formation along a contact that changes from a sharp angular unconformity (Figure 5c) with 10s of m of erosional relief cut on older units in some areas, to a quasi-conformable contact at the top of the fanning-dip interval (Figures 5d and 7). Bow Willow beds also includes a thin algal-laminated limestone at its base in an area northeast of Vallecito Creek, between the June Wash fault in the northwest and View of the Badlands Wash in the southeast (Figure 3). The limestone is ~0.5–1.0 m thick and contains a dense lacey network of mm- to cm-diameter calcareous roots and reed stems typical of a shallow lake or marsh flora (Figure 5e). The limestone is overlain by ~25 m of poorly sorted sandstone, pebbly sandstone and conglomerate with clasts of calcite-cemented sandstone that are reworked from the underlying Hueso Formation (Figure 8). The reworked sandstone clasts display imbrications that indicate transport to the southwest. The Bow Willow beds is capped and truncated at a low angle by a calcic paleo-aridisol characterized by a 20–40 cm thick zone of massive carbonate (sandy calcrete) with thin platey calcite laminae that grades downward to red cemented sandstone with large calcite nodules. Large desiccation cracks penetrate up to ~2 m below stripped surfaces (Figure 5f). The paleosol features suggest stage 3 to stage 4 soil development [*Gile et al.*, 1966; *Machette*, 1985]. Bedding in the Bow Willow beds northeast of Vallecito Creek dips SW ~6°– 8° and is truncated at a very low angle by the more gently dipping (0–5°) capping calcic paleosol and younger Quaternary units.

[16] The age of the Bow Willow beds is estimated where it conformably overlies the fanning-dip interval at the top of the Hueso Formation, 10–20 m above the top of the Jaramillo subchron (Figures 3 and 4). Prior paleomagnetic studies

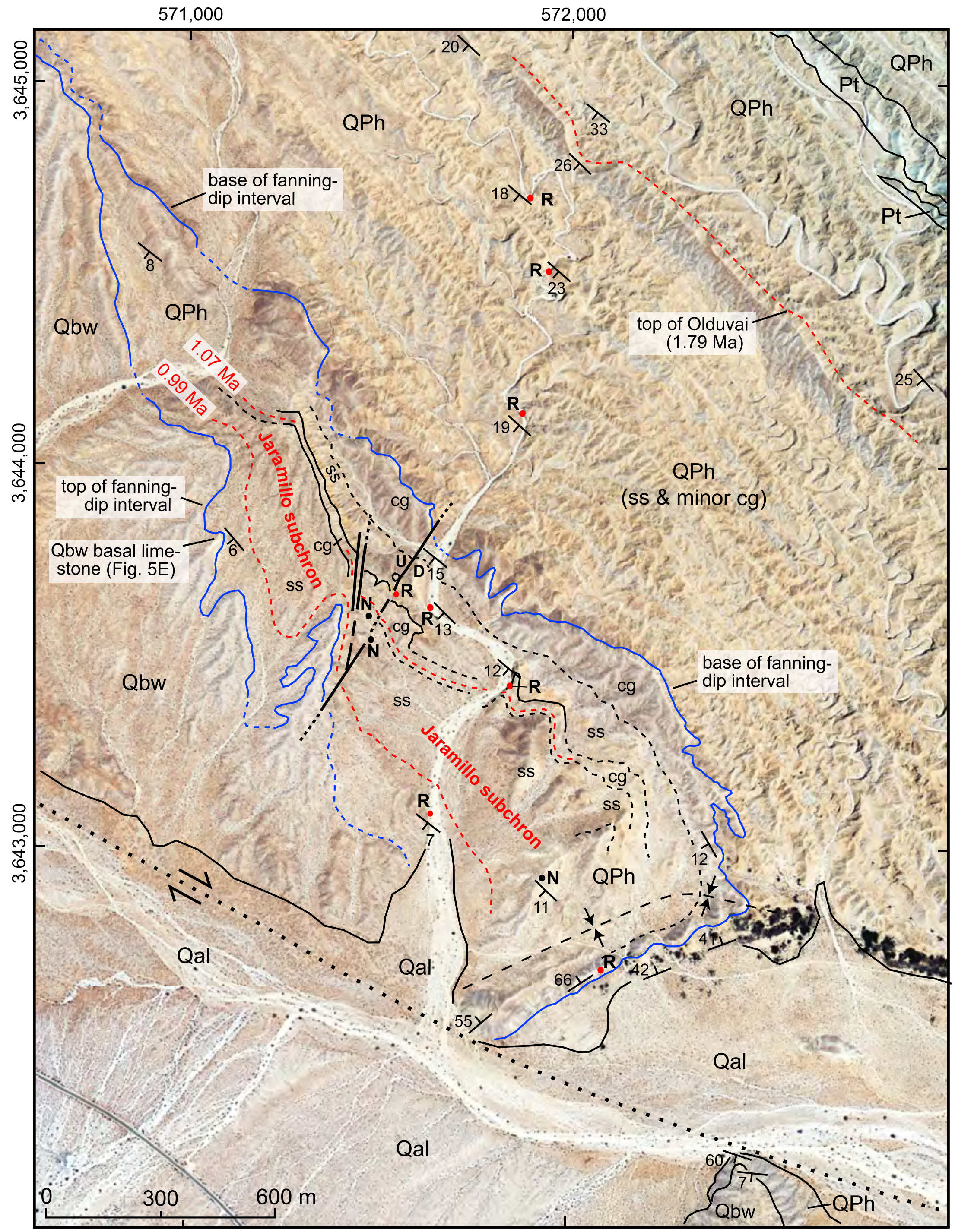

Figure 6. Detailed geologic map showing wedge-shape geometry and age controls for the fanning-dip interval in the upper Hueso Formation. Paleomagnetic sample localities from *Dorsey et al.* [2011]; N is normal and R is reversed polarity. Lithic designators are the same as in Figure 3. Other abbreviations: ss, sandstone; cg, conglomerate. Location shown in Figure 3. UTM coordinates for zone 11S, datum WGS 84.

show that the base of the Bow Willow beds coincides with the top of the Jaramillo subchron (0.99 Ma), and thus is ca. 1.0 Ma (Figures 4 and 7) [*Opdyke et al.*, 1977; *Johnson et al.*, 1983; *Dorsey et al.*, 2011]. The duration of the Bow Willow beds is not known but it likely represents a short period of time (≤ca. 50 kyr) based on its thin nature and lack of major internal breaks. The time represented by the capping mature calcic paleosol is difficult to estimate, but the presence of stage 3 to stage 4 soil features suggests a long period of surface exposure, possibly ∼100–200 kyr or more [e.g., *Gile et al.*, 1966; *Machette*, 1985].

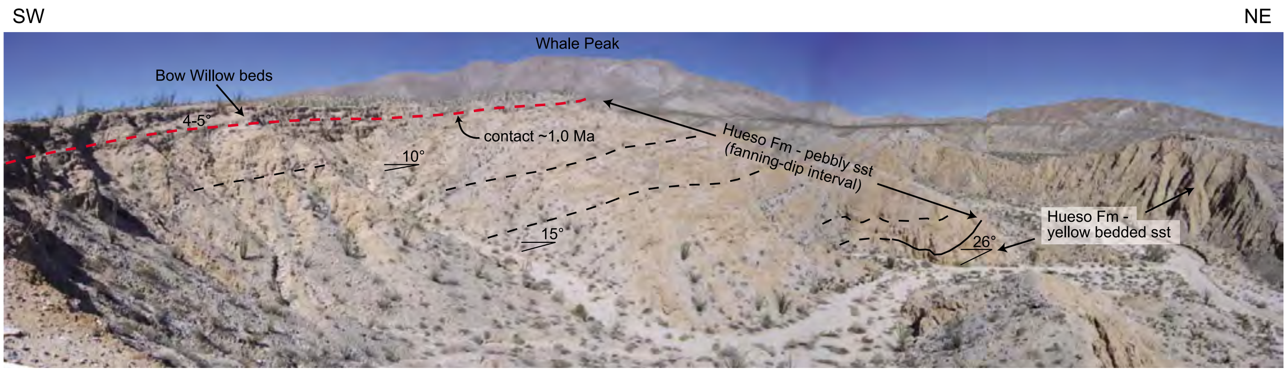

Figure 7. Fanning-dip interval in the upper Hueso Formation and base of overlying Bow Willow beds. See map in Figure 3 for location, south of Whale Peak.

3.4. Paleocurrents

[17] Paleocurrent data were collected from imbricated clasts in basal traction deposits of clast-supported conglomerate beds, with minor additional measurements of current lineations and cross-bedding in sandstone. Transport directions show systematic variations in space and stratigraphic position. Data from the Hueso and uppermost Olla Formation reveal consistent transport to the ESE (Figure 9a). Canebrake Conglomerate in the northern Tierra Blanca Mountains (proximal hanging wall of the detachment fault) reveals overall transport toward the north and NNE (Figure 9b). These deposits contain abundant metamorphic clasts that cannot be derived from the plutonic Tierra Blanca or Inkopa mountains, the current detachment footwall. The most likely source for these clasts is the Laguna Mts. to the west (Figure 2), indicating eastward tectonic transport of ca. 7–8 km in the detachment upper plate after deposition of the conglomerate.

[18] Conglomerate on the eastern flank of the Tierra Blanca Mountains, northwest of Canebrake (Figure 3), records transport toward the northeast (Figure 9c), away from the detachment footwall source. Paleocurrent measurements from the Bow Willow beds in lower June Wash reveal transport toward the southwest, toward the detachment footwall and opposite the direction obtained from older Canebrake Conglomerate northwest of Canebrake (Figures 3 and 8d). Our interpretations of these data are presented in section 5.

4. Structural Geology

[19] Two sets of structures are recognized in the study area: (1) discontinuous, inactive strands of the low-angle West Salton detachment fault; and (2) a complex network of younger, active NW- and NE-striking, steep to vertical strike-slip and oblique-slip faults and related folds (Figure 3). The modern strike-slip faults clearly offset and post-date strands of the older detachment fault. Crosscutting relationships that illustrate the relative age of the two fault systems are well displayed at the north end of the Tierra Blanca Mountains and on the south flank of Whale Peak, where multiple segments of the detachment fault system are truncated and displaced by younger strands of the modern Elsinore and related faults (Figure 3).

[20] The West Salton detachment fault is a regional, normal to oblique-normal low-angle fault that is offset in the study area by a complex set of younger dextral and sinistral strike-slip faults (Figure 3). Dips on the detachment fault in the study area cluster between ~20° and 30° (Figure 10a), with somewhat steeper dips in the breakaway zone. Fault striae indicate hanging wall slip to the east or ESE, with minor modes trending NNE and SSW that likely record flexural slip during post-detachment folding (Figure 10b). Whale Peak occupies the core of an east-trending footwall antiform and represents a primary syn-extensional fault corrugation that likely was accentuated by post-detachment

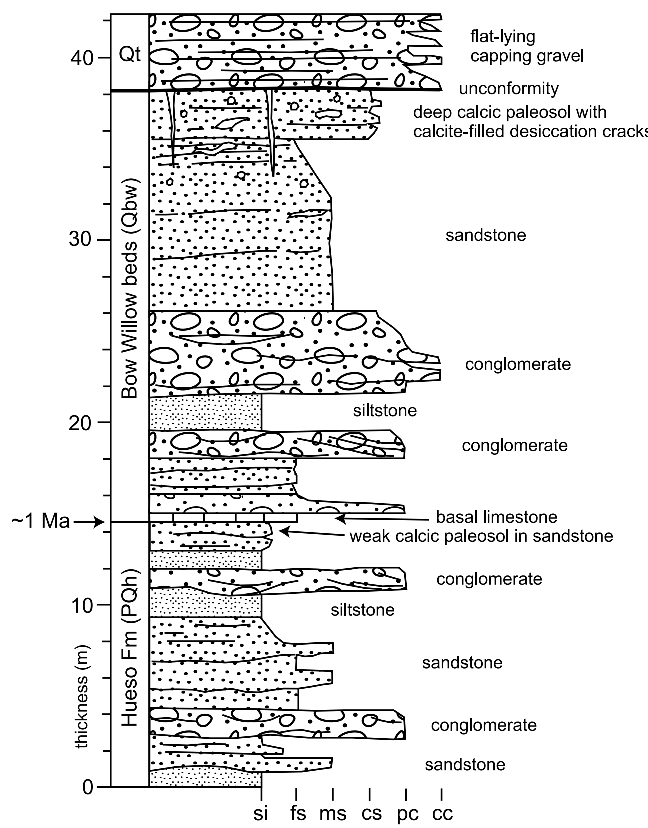

Figure 8. Measured section of uppermost Hueso Formation and overlying Bow Willow beds, southern June Wash (see Figure 3 for location).

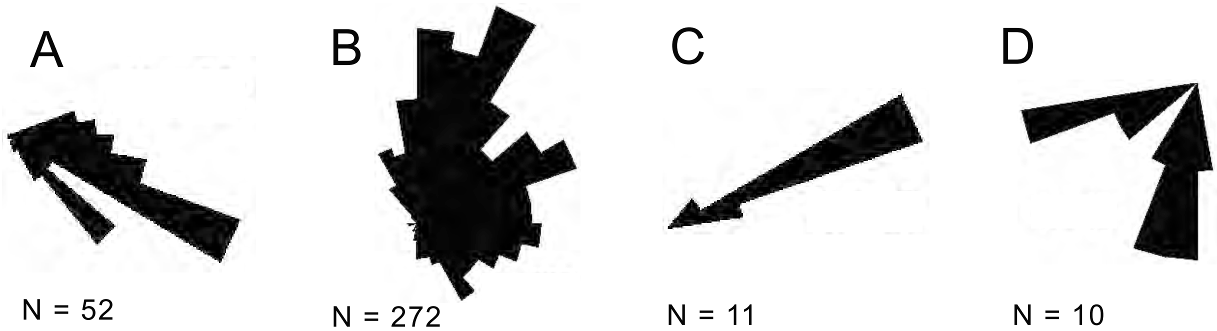

Figure 9. Paleocurrent data from the northwestern Fish Creek–Vallecito basin. Figures 9a–9c are from syn-detachment units (Palm Spring Group), and Figure 9d is from the post-detachment Bow Willow beds. (a) Uppermost Olla and Hueso formations. (b) North end of Tierra Blanca Mountains. (c) Eastern Tierra Blanca Mountains northwest of Canebrake. (d) Bow Willow beds in lower June Wash.

fold growth. South of Whale Peak and north of the Tierra Blanca Mountains, strands of the detachment fault are exposed on the north and south sides of an east- to ESE-trending synform that contains syn-detachment hanging wall deposits of the Hueso Formation and Canebrake Conglomerate (Figure 3). The detachment fault is well exposed west of Canebrake in an oblique dextral-normal breakaway position, where it juxtaposes boulder-bearing Canebrake Conglomerate in the upper plate against highly brecciated tonalite in the footwall (Figures 11a and 11b).

[21] Post-detachment structures in the study area include steep to vertical strike-slip and oblique-slip faults that crosscut and postdate the detachment fault, and a related set of west- to WNW-trending folds (Figure 3). The faults cut all sedimentary units including late Quaternary alluvial fan deposits, and commonly include a narrow zone of clay-rich brittle gouge in the fault core (Figures 11c and 11d). The June Wash fault is a sub-vertical northeast-striking fault with down-on-the northwest offset and ~1 km of dextral separation (Figure 3) that is unusual for NE-striking faults in this area. An ENE-dipping dextral-normal fault on the northeast margin of the Tierra Blanca Mountains offsets an active alluvial fan (Figure 11e), creating a prominent range-front fault scarp that provides evidence for Holocene activity. The south Whale Peak fault truncates and offsets the detachment fault and young alluvial fan deposits, defining prominent fault scarps that record oblique sinistral and down-on-the-SSE displacement. West- to WNW-plunging folds occupy a complex zone of wrench deformation that links the Vallecito and Hapaha Flat faults in the northeast to the Earthquake

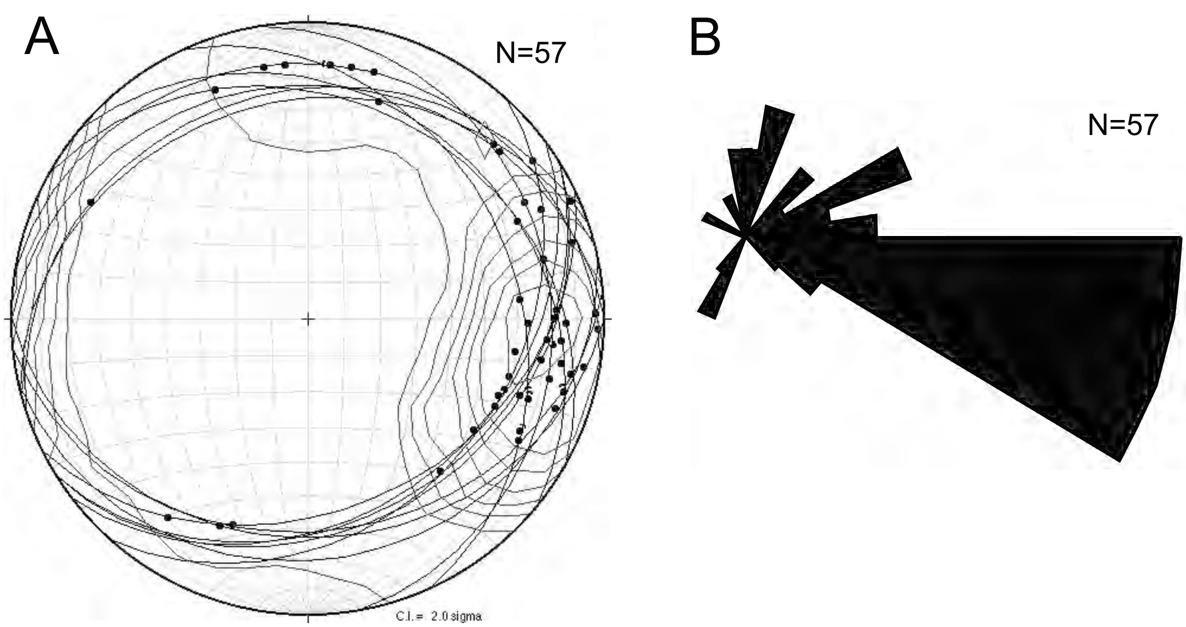

Figure 10. Structural data from the West Salton detachment fault, northwestern Fish Creek–Vallecito basin. (a) Equal area plot showing gentle N, S, and E dips on the detachment fault, reflecting presence of a large synformal corrugation in the study area (Figure 3). Fault striae trends are clustered at 95–100°. (b) Rose diagram showing dominant E to ESE trend of fault striae. Minor modes trending NNE and SSW likely record flexural slip during post-detachment (post-1 Ma) transpression.

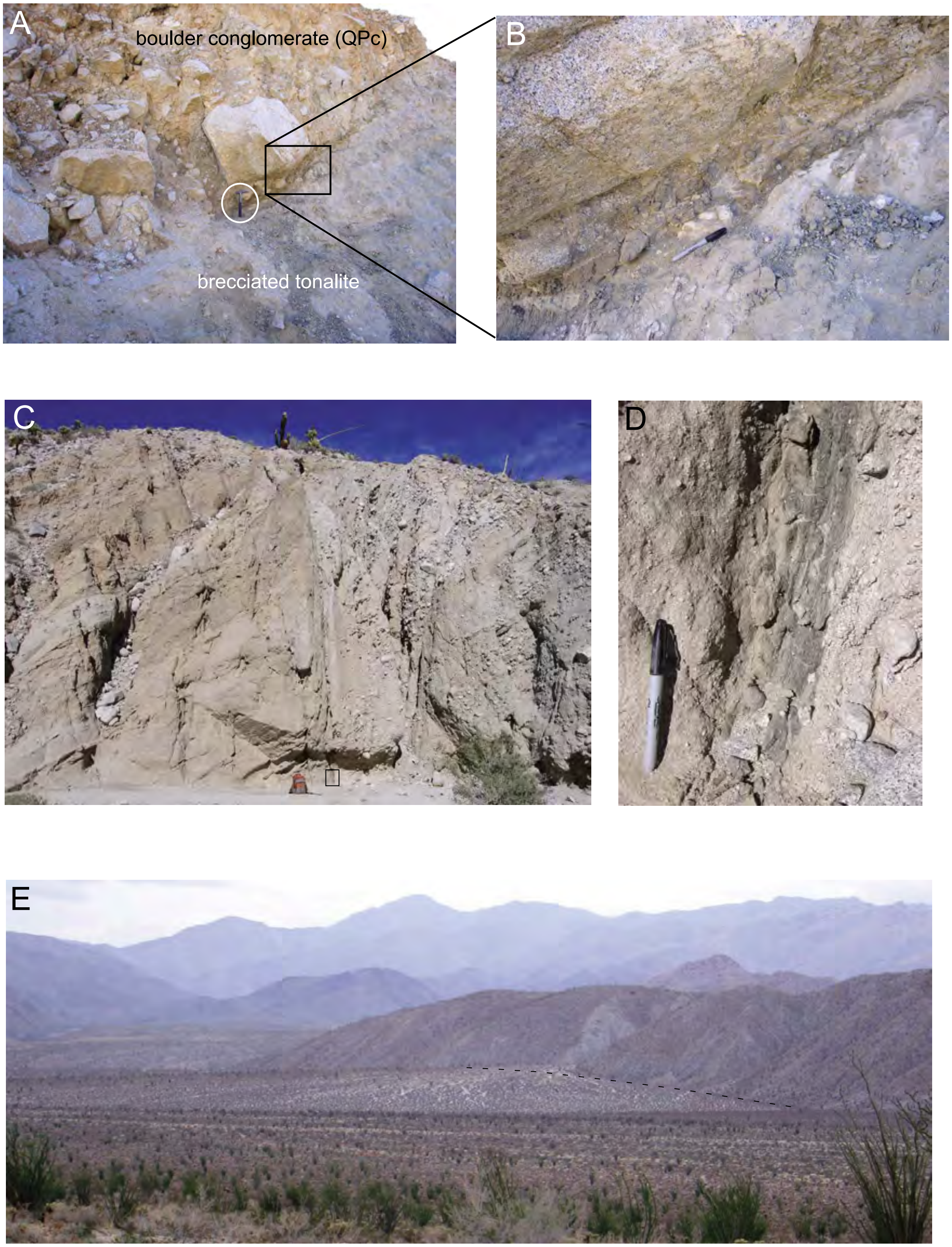

Figure 11. Photographs of faults in the study area. (a) View looking southeast at NE-dipping oblique breakaway zone of the West Salton detachment fault, west of Canebrake. Fault dips 42° NE. (b) Close-up of brittle fault gouge in WSDF. (c) View looking NE along strike at June Wash fault north of the mega-breccia, southeast of Whale Peak (Figure 3). Box shows location of photo in Figure 11d. (d) Close-up of brittle fault gouge in the June Wash fault. (e) View looking SSW at active range-bounding normal fault (dashed line) where it cuts Quaternary alluvial fan on the NE flank of Tierra Blanca Mts. Location is ~4 km SE of the southern edge of Figure 3.

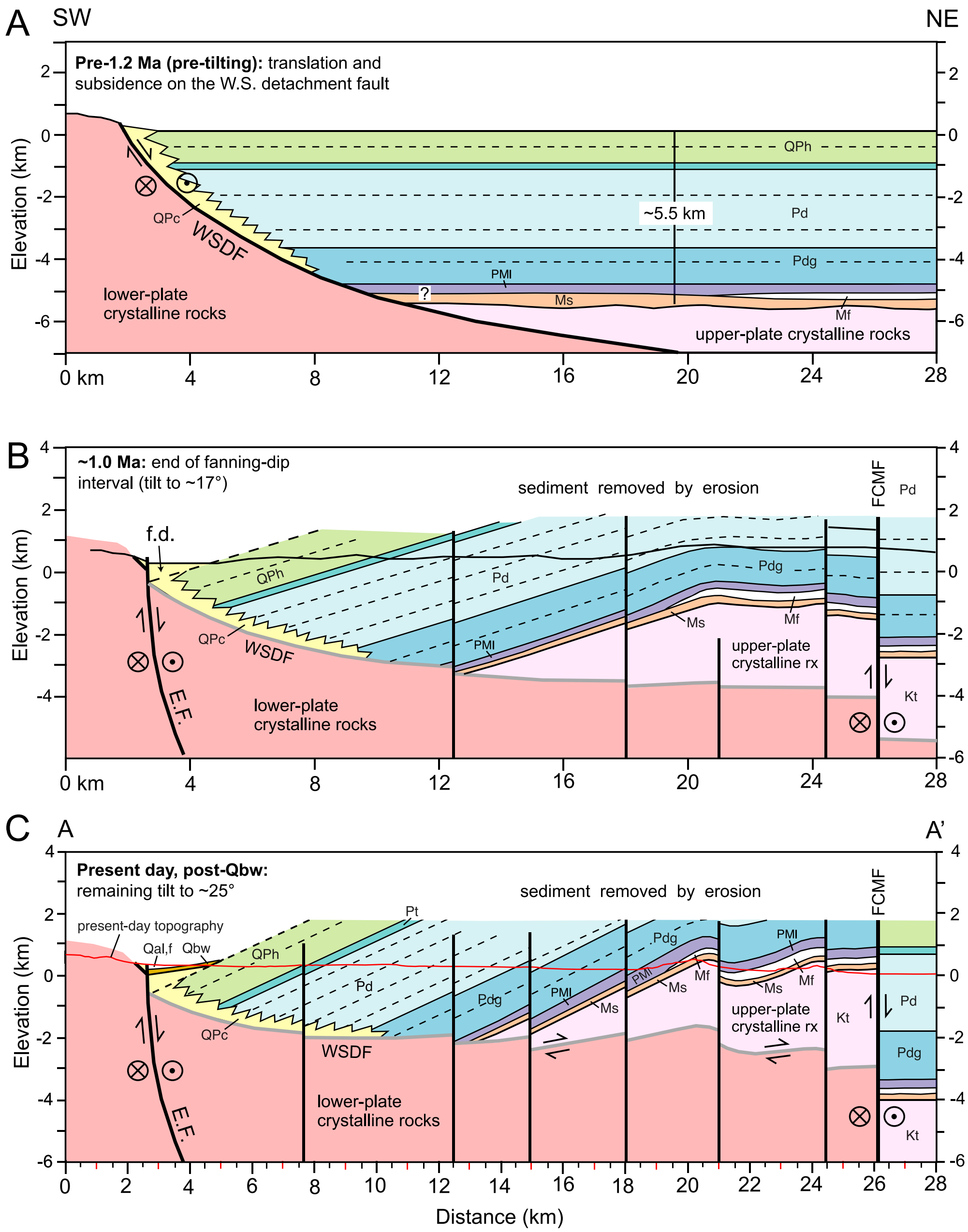

Figure 12. SW-NE cross sections illustrating stages in deformation of the Fish Creek–Vallecito Basin (line of section shown in Figure 2). (a) Translation and subsidence on the WSDF prior to the onset of strike-slip faults and related tilting at 1.2 Ma. (b) End of initial period of tilting at ~1.0 Ma. (c) Present-day cross section. Most faults are steep to vertical, shown here as vertical due to lack of detailed fault-dip data. Lithic designators are same as in Figure 2.

Valley and Elsinore faults in the west (Figure 3). The limited lateral extent and geometry of the folds show that they accommodate local strain gradients and transfer of slip between the Vallecito, Hapaha Flat, June Wash, and south Whale Peak faults.

5. Discussion

[22] The data presented above allow us to reconstruct the end of slip on the West Salton detachment fault and initiation of strike-slip faults in the Fish Creek–Vallecito Basin (Figures 12 and 13). The well-dated stratigraphy provides a high-fidelity record of surficial response to this structural transition. Our work shows that modern strike-slip and oblique-slip faults crosscut, dissect, and postdate the detachment fault and its hanging wall deposits. These active faults and related folds deform all sedimentary units including late Quaternary deposits. In this section we interpret the transition from sedimentation in the detachment hanging wall to uplift and erosion associated with active dextral wrench deformation in the western Salton Trough.

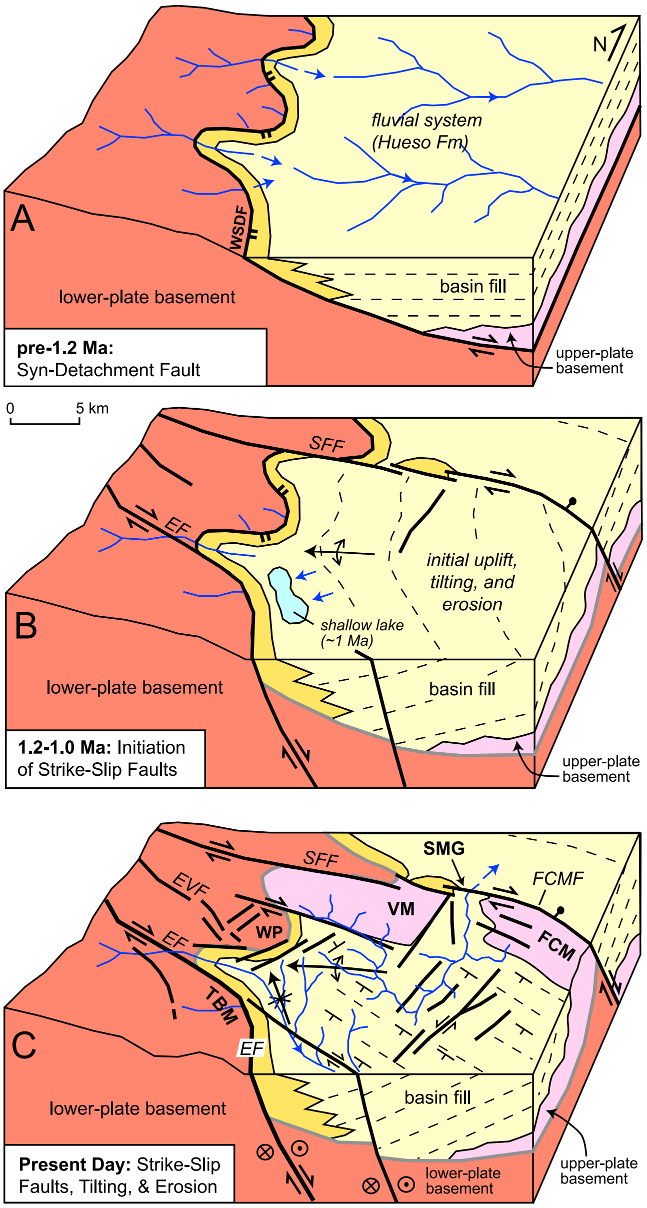

Figure 13. Block diagrams illustrating the structural evolution of the Fish Creek–Vallecito Basin and adjacent areas in the past ∼2 million years. (a) Prior to 1.2 Ma the West Salton detachment fault controlled subsidence at the western margin of the basin. (b) Initiation of strike-slip faults at ∼1.2 Ma caused the onset of intrabasinal tilting, disruption of some local drainages, and formation of a short-lived shallow lake that is represented by the basal limestone of the Bow Willow beds. (c) Present-day configuration with active strike-slip faults and related folds that cause southwestward tilting in a large crustal block bounded by the Elsinore fault on the southwest and the Fish Creek Mountains fault on the northeast. See text for details. EF, Elsinore fault; EVF, Earthquake Valley fault; FCM, Fish Creek Mountains; FCMF, Fish Creek Mountains fault; SFF, San Felipe fault; SMG, Split Mountain Gorge; TBM, Tierra Blanca Mountains; VM, Vallecito Mountains; WP, Whale Peak; WSDF, West Salton detachment fault.

5.1. Syn-Detachment Fault (Pre–1.2 Ma)

[23] The West Salton detachment fault accommodated regional subsidence and basin filling over a large area of the western Salton Trough during Pliocene and early Pleistocene time (Figures 12a and 13a) [e.g., *Axen and Fletcher*, 1998; *Dorsey et al.*, 2011]. During this time, uplift and erosion in the Peninsular Ranges footwall generated a belt of alluvial fans at the basin margin that pass laterally into finer-grained deposits of the supradetachment basin. The lack of fanning dips in hanging wall deposits older than ∼1.2 Ma indicates that slip on the detachment fault beneath the FCVB took place without significant tilting during subsidence in the basin. Top-to-the-ESE slip on the detachment fault generated >8–10 km of horizontal extension and at least 2–4 km of lower plate exhumation between 5 and 2 Ma [*Shirvell et al.*, 2009]. ESE-trending synformal corrugations in the detachment fault formed north and south of the antiform at Whale Peak, funneling fluvial sediments eastward into the basin (Figure 13a).

5.2. Initiation of Strike-Slip Faults (1.2–1.0 Ma)

[24] A short-lived period of syndepositional tilting between ∼1.2 and 1.0 Ma (Figures 12b and 13b) is recorded in the fanning-dip interval in the upper Hueso Formation, which is defined by its distinctive wedge-shape map pattern and up-section decrease in bedding dips (Figure 6). South of Whale Peak the fanning-dip interval is ∼50 m thick and lies directly beneath the ∼1.0-Ma base of the Bow Willow beds with no major unconformities (Figure 7), supporting a young age for the onset of tilting. Bedding dips in the Hueso Formation and older units form the southern limb of a large west-plunging anticline in the north-central part of the map area (Figure 3). This anticline and smaller folds and faults are kinematically linked to transfer of slip between the Vallecito fault in the NE and the Elsinore fault in the SW. Dating of the fanning-dip interval thus allows us to date the onset of fold growth and initiation of strike-slip faults at ca. 1.2 Ma (Figures 12b and 13b).

[25] Although initiation of strike-slip faults caused the onset of intrabasinal tilting and folding at ∼1.2 Ma, it did not produce an immediate end of sedimentation. Instead deposition of the Hueso Formation continued during early tilting, probably across much of the basin, until shortly after the end of the Jaramillo subchron at 0.99 Ma. Sediment accumulation was accommodated by subsidence on the detachment fault which continued slipping until ∼1.0 Ma, as indicated by the young age of conglomerate cut by the detachment on the south flank of Whale Peak (Figures 3 and 4). Thus it appears that both the older detachment fault and the younger strike-slip faults were concurrently active for a short period of time between about 1.2 and 1.0 Ma.

[26] At ca. 1.0 Ma, widespread sedimentation ended and a short-lived shallow lake (basal limestone of the Bow Willow beds) formed in a small structural depression between the Elsinore fault on the southwest and the growing anticline on the northeast (Figure 13b). Formation of this lake in an area of previously throughgoing fluvial transport reflects disruption of local drainages due to creation of new, structurally controlled topography in the basin. Above the limestone, sandstone clasts reworked from the underlying Hueso Formation record transport to the southwest (Figure 9d),

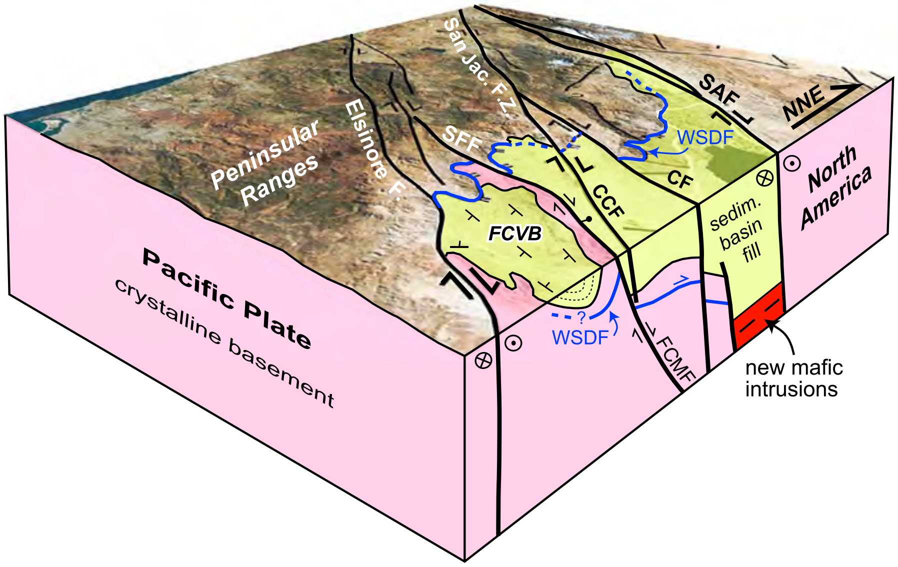

Figure 14. Block diagram showing inferred relationship of faults in the study area to present-day crustal architecture of the southern San Andreas fault system. Inactive strands of the West Salton detachment fault (WSDF) are offset and deformed by the younger Elsinore, San Felipe and San Jacinto faults. CCF, Coyote Creek fault; CF, Clark fault; CPF, Cerro Prieto fault; EF, Elsinore fault; FCVB, Fish Creek–Vallecito Basin; SAF, San Andreas fault; SFF, San Felipe fault.

providing further evidence for disruption and reversal of local drainages. Increased uplift and continued tilting eventually caused the end of deposition and development of the thick calcic paleosol that caps and truncates the Bow Willow beds. Exposure of this surface and resulting soil formation persisted for an unknown duration, perhaps ~100–200 kyr. The relatively thin Bow Willow beds and its capping calcic paleosol thus record the end of slip on the detachment fault, end of widespread sedimentation in the Fish Creek–Vallecito Basin, and transition to the modern regime of active strike-slip faulting, uplift, and erosion.

5.3. Modern Strike-Slip Faults and Crustal Tilting

[27] The present-day structure of the Fish Creek–Vallecito Basin is shown schematically in Figures 12c and 13c. Figure 14 illustrates the regional 3-D crustal architecture and relationship of the study area to the San Andreas and San Jacinto fault zones in the Salton Trough region. The Elsinore and Fish Creek Mountains faults bound a crustal block that measures ~20–25 km across strike, with bedding dips that record overall tilting to the southwest. Southwest tilting of this block has resulted in 5.5–6 km of post-1.2 Ma uplift and exhumation of the base of the section in the Fish Creek Mountains (Figures 2, 12c, 13c, and 14) [*Dorsey et al.*, 2011]. Transpressional folds and faults at the northern margin of the basin define a complex stepover zone that links the Vallecito, Hapaha Flat, June Wash, south Whale Peak, and Earthquake Valley faults (Figure 3). Both the smaller-scale faults and fault-controlled folds, and the larger-scale southwest block tilting, are a direct result of active dextral-wrench deformation that initiated at ~1.2 Ma.

[28] The top of the section is located near the southwest margin of the basin, 1–2 km northeast of the Tierra Blanca Mountains where oblique dextral-normal faults of the Elsinore fault zone have generated prominent fault scarps that cut late Quaternary and Holocene alluvial fans [*Pinault*, 1984; *Magistrale and Rockwell*, 1996; *Todd*, 2004; this study]. Oblique subsidence along these faults controls the modern course of Vallecito Creek and local fault-controlled geomorphology (Figures 3 and 11e). The map pattern clearly shows that older strands of the detachment fault have been cut and replaced by active strands of the Elsinore fault zone.

5.4. Elsinore Fault Slip Rate and Slip Budget

[29] Our results place new constraints on the long-term slip rate for the southern Elsinore fault. Total offset of the western margin of Cretaceous plutons decreases from ~2 km at Granite Mountain to ~1 km at the southeast end of Mason Valley (Figure 2) [*Lampe*, 1988; *Grove et al.*, 2003]. The difference in offset between these two localities likely reflects transfer of slip from the Elsinore fault east to the Earthquake Valley fault. Using 1.1–1.3 Ma for the age of fault initiation [this study] and total offset of 1–2 km, the lifetime slip rate for the Elsinore fault in the study area is 0.8–1.8 km/Myr, or approximately 1–2 mm/yr. This estimate is similar to a late Pleistocene rate of 1.6 ± 0.4 mm/yr that was recently determined from U-series dating of soil carbonate in offset alluvial fans in the Coyote Mountains [*Fletcher et al.*, 2011]. The latter study suggested that slip rate may increase sharply along strike to the northwest based on along-strike increase of offset in the last earthquake, which would be consistent with a previously determined Holocene rate of 3.3–5.5 mm/yr [*Pinault and Rockwell*, 1984]. Our result suggests that 1.6 ± 0.4 mm/yr [*Fletcher et al.*, 2011] may instead be representative of the long-term slip rate on the southern Elsinore fault.

[30] The northern Elsinore fault has a slip rate of ~3–6 mm/yr, determined for timescales ranging from Holocene to Pliocene [*Millman and Rockwell*, 1986; *Vaughan and Rockwell*, 1986; *Hull and Nicholson*, 1992; *Rockwell et al.*,

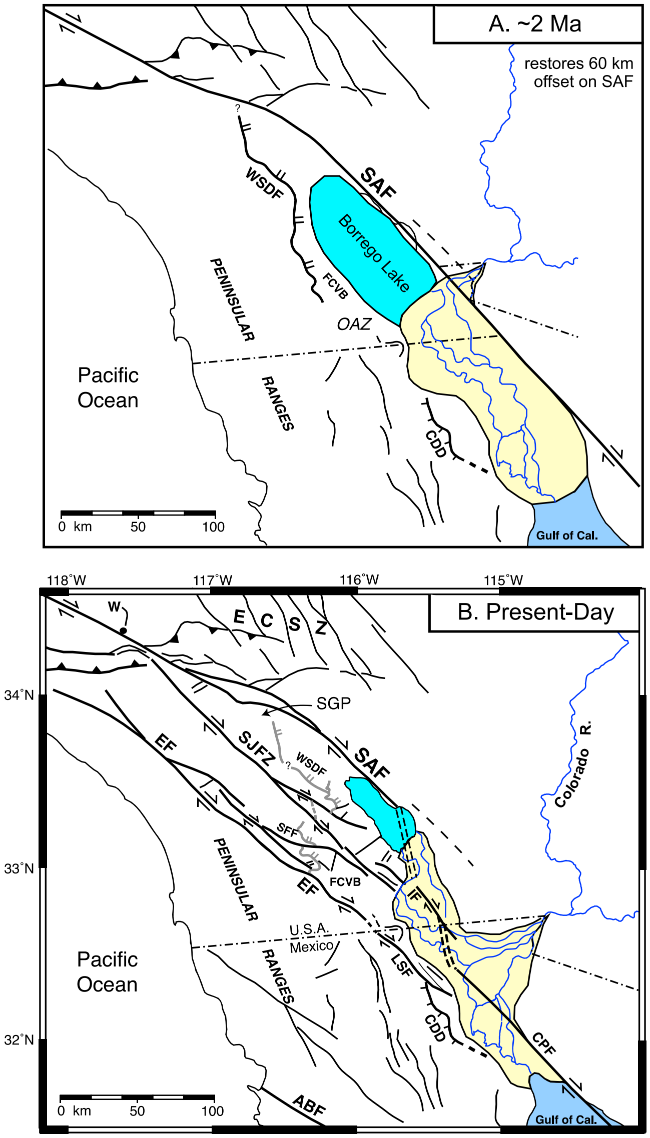

Figure 15. Regional maps showing fault patterns before and after tectonic reorganization of the plate boundary in southern California at ca. 1.2 Ma. (a) Reconstructed faults of the southern San Andreas fault system at ca. 2 Ma, prior to initiation of young strike-slip faults, when the Salton Trough basin was bounded on the west by the low-angle West Salton detachment fault. (b) Present-day fault geometry, modified from Figure 1, showing greatly expanded width and complexity of the San Andreas system compared to pre-1.2 Ma pattern. OAZ, Ocotillo accommodation zone [*Axen*, 1995]; other abbreviations as in Figure 1.

2000], significantly faster than two new estimates for the southern Elsinore fault [*Fletcher et al.*, 2011; this study]. The discrepancy between the northern and southern Elsinore fault (∼3–6 mm/yr in the north; 1–2 mm/yr in the south) can be explained by transfer of slip from the Elsinore fault to the San Felipe and Fish Creek Mountains faults in the east and southeast (Figures 1 and 2) via fault linkages that probably have persisted for the past ca. 1 Myr. Previous workers proposed that the difference in total offset and slip rate is taken up by the Earthquake Valley fault [*Magistrale and Rockwell*, 1996], but limited offset near Whale Peak [*Kairouz*, 2005] makes this interpretation unlikely. Total offset on the San Felipe fault is ∼6 ± 3 km since its initiation at 1.1–1.3 Ma [*Steely et al.*, 2009], representing a lifetime slip rate of roughly 5 ± 3 mm/yr. Thus, despite existing uncertainties, displacement on the San Felipe fault appears sufficient to balance the budget for offset and slip rate between the southern and northern segments of the Elsinore fault, suggesting long-lived transfer of slip from the northern Elsinore fault east to the San Jacinto fault zone in the Salton Trough (Figure 1).

5.5. Tectonic Reorganization of the San Andreas System

[31] Initiation of the Elsinore fault was part of a major tectonic reorganization that profoundly changed the southern San Andreas fault system at ca. 1.2 Ma. Prior studies inferred an age of ∼2–2.5 Ma for the San Jacinto fault based on extrapolation of late Pleistocene slip rates back in time [e.g., *Rockwell et al.*, 1990; *Blisniuk et al.*, 2010], while others concluded from geologic data that the San Jacinto and related faults initiated ∼1.1–1.4 Ma [*Morton and Matti*, 1993; *Lutz et al.*, 2006; *Steely et al.*, 2009; *Janecke et al.*, 2010]. This study shows that the younger age of initiation (∼1.2 Ma) is correct for the Elsinore fault in our study area, and indicates synchronous formation of the Elsinore and San Jacinto fault zones in the western Salton Trough.

[32] Termination of slip on the West Salton detachment fault due to initiation of strike-slip faults is well documented north of the Vallecito Mountains, where the older detachment is offset and strongly deformed by the younger San Felipe fault and related folds (Figure 2) [*Steely et al.*, 2009; *Janecke et al.*, 2010]. In that area conglomerate of the Pleistocene Ocotillo Formation rests in angular unconformity on older syn-detachment deposits, and records filling of a local depression that was formed by new faults in a transpressive stepover of the San Felipe fault zone. Basal gravel of the Ocotillo Formation, well dated at 1.1 Ma, prograded rapidly 35–40 km across the western Salton Trough in response to the onset of rapid uplift and large erosional flux from formerly subsiding proximal parts of the supradetachment basin [*Lutz et al.*, 2006; *Kirby et al.*, 2007]. Initiation of the San Jacinto fault zone at 1.1–1.3 Ma produced broad folding and an angular unconformity across the San Felipe anticline, reorganized stream drainages in the Peninsular Ranges, and created new basin-bounding faults in and around the Borrego Badlands [*Lutz et al.*, 2006; *Dorsey and Roering*, 2006; *Kirby et al.*, 2007; *Janecke et al.*, 2010].

[33] Prior to initiation of strike-slip faults at ∼1.2 Ma, dextral-oblique motion between the Pacific and North America plates was accommodated by linked slip on two major faults: the San Andreas fault on the northeast and the much smaller-offset West Salton detachment fault on the southwest (Figure 15a) [*Axen and Fletcher*, 1998; *Axen*, 2008]. Starting at about 1.2 Ma, new strike-slip faults including the San Jacinto, San Felipe, Earthquake Valley and Elsinore faults cut across and terminated slip on the West Salton detachment fault, expanding the width of the San Andreas fault system to about 80 km (Figure 15b) [*Janecke et al.*, 2010]. As a result of this tectonic reorganization, slip rate on the southern San Andreas fault in Coachella Valley was reduced from a likely value of ∼35 mm/yr

prior to 1.2 Ma (inferred from studies at Wrightwood, Figure 1) [*Humphreys and Weldon*, 1994; *Bennett et al.*, 2004; *Weldon et al.*, 2004] to ~14–17 mm/yr after 1.2 Ma [*Behr et al.*, 2010]. While these rates are based on offset of late Quaternary to Holocene features, it is reasonable to infer that strike-slip motion currently accommodated across the 80 km-wide fault zone was focused on the San Andreas fault prior to initiation of the Elsinore, San Jacinto and San Felipe faults.

5.6. Implications for Fault Zone Evolution

[34] The regional tectonic reorganization documented in this and other recent studies provides a useful example for comparison to other case studies and models of strike-slip fault zone evolution. Compilations of fault data show that geometric complexity generally decreases with increased fault offset, suggesting that progressive accumulation of displacement works to remove fault discontinuities, smooth the fault plane, and reduce geometric complexity through time [*Wesnousky*, 1988, 1990; *Stirling et al.*, 1996]. *Cowgill et al.* [2004] found that localized asymmetric shortening at the inside corners of a double restraining bend on the Altyn Tagh fault caused the principal fault trace to undergo vertical-axis rotation during deformation. They inferred that rotation of the fault plane decreased the bend angle and smoothed the fault trace over time, and suggested that this may be a general mechanism for simplification of strike-slip faults through time. In contrast, progressive deformation along the southern San Andreas fault led to an abrupt *increase* in fault zone complexity by creation of a new set of strike-slip faults that substantially widened the fault system (Figure 15). The discrepancy between model predictions and evolution of the San Andreas fault zone probably reflects additional complicating factors such as pre-existing fault geometries and topography, crustal thickening and loading by oblique convergence, and growth of an impinging antithetic fault that deflected the main fault trace over time.

[35] The San Jacinto, Elsinore and related strike-slip faults are believed to have initiated as a result of oblique convergence, transpressive deformation and increased resistance to strike-slip motion through the San Gorgonio Pass restraining stepover in early Pleistocene time (Figures 1 and 15) [*Matti et al.*, 1985; *Matti and Morton*, 1993; *Morton and Matti*, 1993; *Langenheim et al.*, 2004]. The San Gorgonio Pass stepover is a complicated network of multiple branching and intersecting transpressional faults with a complex pattern of topography and uplift [*Spotila et al.*, 1998, 2002; *Spotila and Sieh*, 2000; *Yule and Sieh*, 2003]. The 15-km wide restraining stepover is postulated to have formed by progressive deflection of the San Andreas fault by left-lateral slip on the Pinto Mountain fault and transrotation of blocks in the eastern Transverse Ranges [*Matti and Morton*, 1993; *Spotila and Sieh*, 2000]. Uplift of the San Bernardino Mountains at this time took place on southwest-directed transpressional faults in San Gorgonio Pass and north-directed thrusts along the northern San Bernardino Mountains, causing increased erosion and rapid transport of coarse clastic sediment to the north and south away from the zone of growing topography [*Meisling and Weldon*, 1989; *Spotila and Sieh*, 2000]. Stratigraphic and paleomagnetic studies in several locations show that the base of these coarse deposits is ~1.4–1.7 Ma [*Meisling and Weldon*, 1989; *Morton and Matti*, 1993; *Albright*, 1999; *Cox et al.*, 2003], slightly older than the well dated age of the San Jacinto and Elsinore faults in the western Salton Trough (ca. 1.2 Ma). *Morton and Matti* [1993] and *Matti and Morton* [1993] concluded from stratigraphic data in the San Timoteo Badlands, west of San Gorgonio Pass, that the northern Jacinto fault initiated at ca. 1.2–1.5 Ma.

[36] The slight age difference between stratigraphic signals near the San Bernardino Mountains and in the western Salton Trough has two possible explanations: (1) the northern San Jacinto fault first formed at ~1.5 Ma near San Gorgonio Pass and took up to ~0.3 Myr to propagate southeast into the western Salton Trough; or (2) uplift in the San Bernardino Mountains was driven by transpressive deformation that preceded initiation of the San Jacinto and Elsinore fault systems, which are the same age (~1.2 Ma) along their entire length. Existing data are not sufficient to distinguish between these hypotheses, which need not be mutually exclusive. Precise ages of initiation of the northern San Jacinto and Elsinore faults, and of the southern Elsinore system in northern Mexico, are needed to test these hypotheses and better understand the patterns of fault initiation and propagation in the southern San Andreas fault system.

[37] The first hypothesis above (southeastward fault propagation) is supported by relations in the sierras Cucapah and El Mayor in the southern Elsinore-Laguna Salada fault system (Figure 1), which suggest that strike-slip faults there may be quite young. The Laguna Salada fault cut and deactivated the west-vergent Cañada David detachment in the Laguna Salada area geologically recently [*Isaac*, 1987; *Axen and Fletcher*, 1998; *Dorsey and Martín-Barajas*, 1999], though precise age constraints are lacking. The Cañada David detachment was active during roughly the same time as the West Salton detachment [*Axen and Fletcher*, 1998; *Axen et al.*, 2000] and was separated from it by the poorly understood Ocotillo accommodation zone [*Axen*, 1995] which is now overprinted by the linked southern Elsinore and northern Laguna Salada faults. The Laguna Salada fault is a NW-striking oblique dextral fault that bounds the SW side of the Sierra Cucapah and transfers some slip southward onto the NE-striking Cañon Rojo normal fault [*Mueller and Rockwell*, 1995, *Dorsey and Martín-Barajas*, 1999]. Several other NW-striking dextral faults also cut the range [*Barnard*, 1968; *Gastil and Fenby*, 1991; *Fletcher and Spelz*, 2009]. Farther south, in the Sierra El Mayor, the Cañada David detachment was active into late Pleistocene time [*Axen et al.*, 1999; *Spelz et al.*, 2008; *Fletcher and Spelz*, 2009], and thus is concurrently active with dextral faults in the region. Concurrent activity on the southern Cañada David detachment and the strike-slip faults, and the strongly oblique nature of the Laguna Salada fault, suggest that the dextral system in northern Baja California is not yet well integrated and is relatively juvenile, perhaps recording post-1.2 Ma propagation of the Elsinore-Laguna Salada fault system into Mexico. Alternatively, the detachment and strike-slip fault systems may have been concurrently active since Pliocene or late Miocene time, as suggested by *Fletcher and Spelz* [2009]. Uncertainty in the age of the Laguna Salada fault limits our ability to assess the first hypothesis.

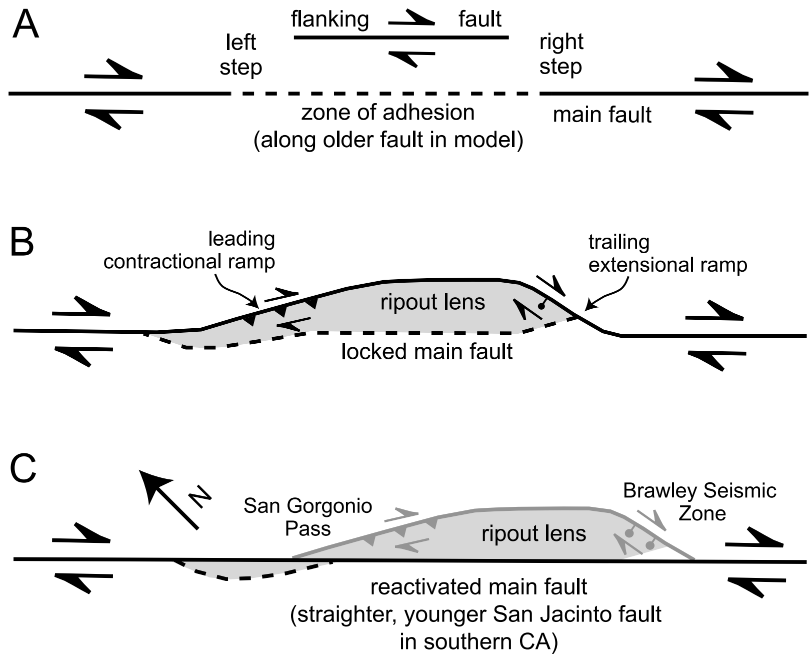

Figure 16. Geometrical model for evolution of a sidewall ripout along a strike-slip fault, modified from *Swanson* [2005]. (a) Adhesion and sticking causes part of the main fault to become locked, forcing creation of a new flanking fault. (b) The flanking fault links to the main fault via releasing and restraining bends, and the ripout lens becomes partially deformed and translated during fault offset. (c) The main fault is reactivated, the flanking fault segment is abandoned, and a detached slice of the ripout lens at the leading ramp is further translated along the active fault trace. Fault geometries in the sidewall-ripout model resemble those of the southern San Andreas system (Figure 1, labels in Figure 16c), but the timing of fault development in southern California is different than that predicted by the model. See text for discussion.

[38] The second hypothesis (simultaneous fault initiation) is consistent with deformation patterns one might expect to result from oblique convergence across San Gorgonio Pass. Broad uplift in the San Bernardino Mountains starting ~1.5 Ma was produced by slip on crustal-scale thrust faults in response to oblique convergence across the San Andreas fault zone [*Meisling and Weldon*, 1989; *Spotila and Sieh*, 2000]. Prior to that, the San Jacinto and Santa Rosa mountains were exhumed and uplifted in the footwall of the West Salton detachment fault from latest Miocene (?) to early Pleistocene time [*Axen and Fletcher*, 1998; *Matti et al.*, 2002, 2006]. We infer that oblique collision of the high-standing detachment footwall (strong Peninsular Ranges beam) with the topographically lower southern San Bernardino Mountains thrust belt may have induced strong horizontal compressive stresses that ultimately exceeded the strength of the Peninsular Ranges crust. These stresses may have been relieved by formation of the San Jacinto and Elsinore fault systems, which allowed southeastward lateral escape of Peninsular Ranges blocks between the San Jacinto and southern San Andreas faults [e.g., *Langenheim et al.*, 2004].

[39] One provocative model for strike-slip fault evolution postulates that adhesion and sticking on a master fault cause it to become locked, forcing creation of a new flanking fault that links to the master fault via releasing and restraining bends to form a lenticular “sidewall ripout” (Figure 16) [*Swanson*, 1989, 2005]. Continental strike-slip fault zones commonly include paired restraining and releasing bends or stepovers that bound regional sidewall ripouts in various stages of development [*Wakabayashi et al.*, 2004; *Mann*, 2007]. The southern San Andreas system has the geometry of a classic sidewall ripout bounded on the northeast and southwest by the San Andreas and Elsinore and faults, on the southeast by the Brawley and Mexicali seismic zones, and on the northwest by the San Gorgonio Pass restraining bend and western Transverse Ranges (Figure 1), inviting comparison to the sidewall-ripout model [e.g., *Mann*, 2007].

[40] The model predicts that sidewall ripouts form when a segment of a relatively straight master strike-slip fault becomes locked due to adhesion (rather than geometric complexities), abandoned for a period of time with slip transferred to a parallel fault, and is later reactivated (Figure 16) [*Swanson*, 2005]. The geometry of the southern San Andreas and San Jacinto fault zones is similar to that predicted by this model, but the younger and straighter San Jacinto fault zone occupies the position of the original master fault in the model. Thus the sidewall-ripout model does not correctly predict the documented evolution of the southern San Andreas fault system. Similar geometric and timing problems arise when the San Andreas, San Jacinto and Elsinore fault systems are all considered.

[41] We postulate that the new (San Jacinto, Elsinore) faults are favored because they provide a straighter and more efficient path for strain accumulation than the circuitous trace of the southern San Andreas fault [e.g., *Li and Liu*, 2006]. Although the fault system is now more complex than it was before initiation of new strike-slip faults at 1.2 Ma, the

reorganization may ultimately result in bypassing and abandonment of the southern San Andreas fault. For example, the southernmost segment of the southern San Andreas fault, the Sand Hills–Algodones fault SE of the Brawley seismic zone (Figure 1), appears to have been largely abandoned already. The slip rate on the San Andreas fault between San Gorgonio Pass and the Brawley seismic zone has decreased since formation of the San Jacinto fault, and this part of the San Andreas may be abandoned in the future. Such a scenario could lead to eventual simplification of the plate-boundary fault zone, consistent with models for smoothing of strike-slip faults through time [e.g., *Wesnousky*, 1988].

6. Conclusions

[42] A complex network of active strike-slip faults and related transpressional folds crosscuts and post-dates the Plio-Pleistocene West Salton detachment fault at the western and northern margins of the Fish Creek–Vallecito Basin. Initiation of the strike-slip faults and folds produced a short-live period of intrabasinal tilting that is recorded in a fanning-dip interval dated between ~1.2 and 1.0 Ma at the top of the Hueso Formation. Because the detachment fault cuts proximal deposits as young as ~1 Ma, we infer that both fault sets were active concurrently for a short time between about 1.2 and 1.0 Ma.

[43] In the overlying Bow Willow beds, a thin basal lacustrine limestone and sandstone clasts reworked from the Hueso Formation record reorganization of local drainages in response to earliest basin inversion, tilting and erosion. The end of subsidence and sediment accumulation shortly after 1 Ma led to formation of a deep calcic paleosol that caps and truncates the Bow Willow beds at a low angle. Since then the Fish Creek Vallecito basin has been uplifted, deeply eroded, and tilted to the southwest in a large crustal block bounded by the Elsinore fault on the southwest and the Fish Creek Mountains fault on the northeast.

[44] Total offset of ~1–2 km on the Elsinore fault yields a lifetime slip rate of about 1–2 mm/yr, similar to late Pleistocene slip rate in the Coyote Mountains (1.6 ± 0.4 mm/yr) and significantly slower than slip rate on the northern Elsinore fault (~3–6 mm/yr). The discrepancy between the northern and southern Elsinore fault likely reflects transfer of slip from the northern Elsinore fault east to the San Felipe fault, which links to the San Jacinto fault zone in the Salton Trough.

[45] Strike-slip faults in the Fish Creek–Vallecito Basin belong to a network of active faults that emerged during a short time interval (~1.1–1.3 Ma) over a large area of the western Salton Trough. These events mark a regional tectonic reorganization that profoundly transformed the geometry, kinematics, and distribution of plate-boundary faults in southern California. The change is not readily explained by existing models for the evolution of strike-slip faults, though it may eventually lead to smoothing and simplification of the plate boundary in southern California. Our results support a growing consensus on the timing and significance of this transition, and highlight the importance of geologic mapping integrated with stratigraphic and structural analysis for understanding the structural histories of tectonically complex, active settings.

[46] **Acknowledgments.** This study was funded by the National Science Foundation (grants EAR-0711293 and EAR-0838119 to Dorsey; EAR-0809638 to Axen) and a Geological Society of America Grant-in-Aid to Peryam. The paper benefited from careful reviews by Nathan Niemi, Todd Ehlers, and an anonymous reviewer. We thank George Jefferson of Anza-Borrego Desert State Park for helpful discussions and permits for field work. Mike Oskin, Susanne Janecke, and Bernie Housen engaged in thoughtful discussions about faulting and sedimentation in the study area. Susanne Janecke is thanked for sharing her preliminary observations and map of the fanning-dip interval. Burnie and Karen Burnworth provided much appreciated lodging and hospitality in Canebrake.

References

Albright, L. B. (1999), Magnetostratigraphy and biochronology of the San Timoteo Badlands, southern California, with implications for local Pliocene–Pleistocene tectonic and depositional patterns, *Geol. Soc. Am. Bull.*, *111*, 1265–1293, doi:10.1130/0016-7606(1999)111<1265:MABOTS>2.3.CO;2.

Axen, G. J. (1995), Extensional segmentation of the main Gulf escarpment, Mexico and United States, *Geology*, *23*, 515–518, doi:10.1130/0091-7613(1995)023<0515:ESOTMG>2.3.CO;2.

Axen, G. J. (2008), A brief overview of Cenozoic extensional tectonism in western North America, in *Ores and Orogenesis: Circum-Pacific Tectonics, Geologic Evolution, and Ore Deposits*, edited by J. E. Spencer and S. R. Titley, *Arizona Geol. Soc. Digest*, *22*, 397–407.

Axen, G. J., and J. M. Fletcher (1998), Late Miocene-Pleistocene extensional faulting, northern Gulf of California, Mexico and Salton Trough, California, *Int. Geol. Rev.*, *40*, 217–244, doi:10.1080/00206819809465207.

Axen, G. J., J. M. Fletcher, E. Cowgill, M. Murphy, P. Kapp, I. MacMillan, E. Ramos Velazquez, and J. Aranda Gomez (1999), Range-front fault scarps of the Sierra El Mayor, Baja California: Formed above an active low-angle normal fault?, *Geology*, *27*, 247–250, doi:10.1130/0091-7613(1999)027<0247:RFFSOT>2.3.CO;2.

Axen, G. J., M. Grove, D. Stockli, O. M. Lovera, D. A. Rothstein, J. M. Fletcher, K. Farley, and P. L. Abbott (2000), Thermal evolution of Monte Blanco dome: Low-angle normal faulting during Gulf of California rifting and late Eocene denudation of the eastern Peninsular Ranges, *Tectonics*, *19*, 197–212, doi:10.1029/1999TC001123.

Barnard, F. L. (1968), Structural geology of the Sierra de los Cucapas, northeastern Baja California, and Imperial County, California, PhD thesis, 157 pp., Univ. of Colo. at Boulder, Boulder.

Behr, W. M., et al. (2010), Uncertainties in slip rate estimates for the Mission Creek strand of the southern San Andreas fault at Biskra Palms Oasis, southern California, *Geol. Soc. Am. Bull.*, *122*, 1360–1377, doi:10.1130/B30020.1.

Bennett, R., W. Rodi, and R. Reilinger (1996), Global Positioning System constraints on fault slip rates in southern California and northern Baja, Mexico, *J. Geophys. Res.*, *101*, 21,943–21,960, doi:10.1029/96JB02488.

Bennett, R. A., A. M. Friedrich, and K. P. Furlong (2004), Codependent histories of the San Andreas and San Jacinto fault zones from inversion of fault displacement rates, *Geology*, *32*, 961–964, doi:10.1130/G20806.1.

Blisniuk, K., T. Rockwell, L. A. Owen, M. Oskin, C. Lippincott, M. W. Caffee, and J. Dortch (2010), Late Quaternary slip rate gradient defined using high-resolution topography and ^{10}Be dating of offset landforms on the southern San Jacinto Fault zone, California, *J. Geophys. Res.*, *115*, B08401, doi:10.1029/2009JB006346.

Cassiliano, M. J. (1999), Biostratigraphy of Blancan and Irvingtonian mammals in the Fish Creek-Vallecito section, southern California, and a review of the Blancan-Irvingtonian boundary, *J. Vertebr. Paleontol.*, *19*, 169–186, doi:10.1080/02724634.1999.10011131.

Cowgill, E., A. Yin, J. R. Arrowsmith, W. X. Feng, and Z. Shuanhong (2004), The Akato Tagh bend along the Altyn Tagh fault, northwest Tibet 1: Smoothing by vertical-axis rotation and the effect of topographic stresses on bend-flanking faults, *Geol. Soc. Am. Bull.*, *116*, 1423–1442, doi:10.1130/B25359.1.

Cox, B. F., J. W. Hillhouse, and L. A. Owen (2003), Pliocene and Pleistocene evolution of the Mojave River, and associated tectonic development of the Transverse Ranges and Mojave Desert, based on borehole stratigraphy studies and mapping of landforms and sediments near Victorville, California, in *Paleoenvironments and Paleohydrology of the Mojave and Southern Great Basin Deserts*, edited by Y. Enzel, S. G. Wells, and N. Lancaster, *Spec. Pap. Geol. Soc. Am.*, *368*, 1–42.

Cox, D. P., R. J. Miller, and K. L. Woodbourne (2006), The Laramide Mesa Formation and the Ojo de Agua Caldera, Southeast of the Cananea Copper Mining District, Sonora, Mexico, *U.S. Geol. Surv. Sci. Invest. Rep.*, *2006-5022*, 7 pp.

Dibblee, T. W., Jr. (1996), Stratigraphy and tectonics of the Fish Creek–Vallecito Mountains, Vallecito Badlands, Coyote Mountains, and Yuha Desert, southwestern Imperial basin, California, in *Sturzstroms and Detachment Faults, Anza-Borrego Desert State Park, California*, *Annu. Field Trip Guideb.*, vol. 24, edited by P. L. Abbott and D. C. Seymore, pp. 59–79, S. Coast Geol. Soc., Santa Ana, Calif.

Dorsey, R. J., and B. A. Burns (1994), Regional stratigraphy, sedimentology and tectonic significance of Oligocene-Miocene sedimentary and volcanic rocks, northern Baja California, Mexico, *Sediment. Geol.*, *88*, 231–251, doi:10.1016/0037-0738(94)90064-7.

Dorsey, R. J., and A. Martín-Barajas (1999), Sedimentation and deformation in a Pliocene-Pleistocene transtensional supradetachment basin, Laguna Salada, Northwest Mexico, *Basin Res.*, *11*, 205–221, doi:10.1046/j.1365-2117.1999.00096.x.

Dorsey, R. J., and J. J. Roering (2006), Quaternary landscape evolution in the San Jacinto fault zone, Peninsular Ranges of southern California: Transient response to strike-slip fault initiation, *Geomorphology*, *73*(1–2), 16–32, doi:10.1016/j.geomorph.2005.06.013.

Dorsey, R. J., A. Fluette, K. A. McDougall, B. A. Housen, S. U. Janecke, G. J. Axen, and C. R. Shirvell (2007), Chronology of Miocene-Pliocene deposits at Split Mountain Gorge, southern California: A record of regional tectonics and Colorado River evolution, *Geology*, *35*, 57–60, doi:10.1130/G23139A.1.

Dorsey, R. J., B. A. Housen, S. U. Janecke, C. M. Fanning, and A. L. F. Spears (2011), Stratigraphic record of basin development within the San Andreas fault system: Late Cenozoic Fish Creek-Vallecito basin, southern California, *Geol. Soc. Am. Bull.*, *123*, 771–793, doi:10.1130/B30168.1.

Fialko, Y. (2006), Interseismic strain accumulation and the earthquake potential on the southern San Andreas fault system, *Nature*, *441*, 968–971, doi:10.1038/nature04797.

Fletcher, J. M., and R. M. Spelz (2009), Patterns of Quaternary deformation and rupture propagation associated with an active low-angle normal fault, Laguna Salada, Mexico: Evidence of a rolling hinge?, *Geosphere*, *5*, 385–407, doi:10.1130/GES00206.1.

Fletcher, K. E., T. K. Rockwell, and W. D. Sharp (2011), Late Quaternary slip rate of the southern Elsinore fault, Southern California: Dating offset alluvial fans via ^{230}Th/U on pedogenic carbonate, *J. Geophys. Res.*, *116*, F02006, doi:10.1029/2010JF001701.

Gastil, R. G., and S. S. Fenby (1991), Detachment faulting as a mechanism for tectonically filling the Gulf of California during dilation, in *The Gulf and Peninsular Provinces of the Califonias*, edited by J. P. Dauphin and B. R. T. Simoneit, *AAPG Mem.*, *47*, 371–375.

Gile, L. H., F. F. Peterson, and R. B. Grossman (1966), Morphological and genetic sequences of carbonate accumulation in desert soils, *Soil Sci.*, *101*, 347–360, doi:10.1097/00010694-196605000-00001.

Grove, M., O. Lovera, and M. Harrison (2003), Late Cretaceous cooling of the east-central Peninsula Ranges batholith (33°N): Relationship to La Posta pluton emplacement, Laramide shallow subduction, and forearc sedimentation, in *Tectonic Evolution of Northwestern Mexico and the Southwestern USA*, edited by S. E. Johnson et al., *Spec. Pap. Geol. Soc. Am.*, *374*, 355–379.

Hull, A. G. (1990), Seismotectonics of the Elsinore-Temecula trough, E1sinore fault zone, southern California, PhD thesis, 233 pp., Univ. of California, Santa Barbara.

Hull, A. G., and C. Nicholson (1992), Seismotectonics of the northern E1sinore fault zone, southern California, *Bull. Seismol. Soc. Am.*, *82*, 800–818.

Humphreys, E. D., and R. J. Weldon (1994), Deformation across the western United States: A local determination of Pacific-North American transform deformation, *J. Geophys. Res.*, *99*, 19,975–20,010, doi:10.1029/94JB00899.

Isaac, S. (1987), Geology and structure of the Yuha Desert between Ocotillo, California, U.S.A., and Laguna Salada, Baja California, Mexico, MS thesis, 165 pp., San Diego State Univ., San Diego, Calif.

Janecke, S. U., R. J. Dorsey, A. N. Steely, S. M. Kirby, A. T. Lutz, B. A. Housen, B. Belgarde, V. Langenheim, T. Rittenour, and D. Forand (2010), High geologic slip rates since Early Pleistocene initiation of the San Jacinto and San Felipe fault zones in the San Andreas fault system: Southern California, USA, *Spec. Pap. Geol. Soc. Am.*, *475*, 48 pp.

Johnson, N. M., C. B. Officer, N. D. Opdyke, G. D. Woodard, P. K. Zeitler, and E. H. Lindsay (1983), Rates of late Cenozoic tectonism in the Vallecito-Fish Creek basin, western Imperial Valley, *Calif. Geol.*, *11*, 664–667.

Kairouz, M. E. (2005), Geology of the Whale Peak region of the Vallecito Mountains: Emphasis on the kinematics and timing of the West Salton detachment fault, southern California, MS thesis, 166 pp., Univ. of Calif., Los Angeles.

Kirby, S. M., S. U. Janecke, R. J. Dorsey, B. A. Housen, V. Langenheim, K. McDougall, and A. N. Steely (2007), Pleistocene Brawley and Ocotillo formations: Evidence for initial strike-slip deformation along the San Felipe and San Jacinto fault zones, southern California, *J. Geol.*, *115*, 43–62, doi:10.1086/509248.

Lampe, C. M. (1988), Geology of the Granite Mountain area: Implications of the extent and style of deformation along the southeast portion of the Elsinore fault, MS thesis, 150 pp., San Diego State Univ., San Diego, Calif.

Langenheim, V. E., R. C. Jachens, D. M. Morton, R. W. Kistler, and J. C. Matti (2004), Geophysical and isotopic mapping of preexisting structures that influenced the location and development of the San Jacinto fault zone, southern California, *Geol. Soc. Am. Bull.*, *116*, 1143–1157, doi:10.1130/B25277.1.

Li, Q., and M. Liu (2006), Geometrical impact of the San Andreas fault on stress and seismicity in California, *Geophys. Res. Lett.*, *33*, L08302, doi:10.1029/2005GL025661.

Lutz, A. T., R. J. Dorsey, B. A. Housen, and S. U. Janecke (2006), Stratigraphic record of Pleistocene faulting and basin evolution in the Borrego Badlands, San Jacinto fault zone, southern California, *Geol. Soc. Am. Bull.*, *118*, 1377–1397, doi:10.1130/B25946.1.

Machette, M. N. (1985), Calcic soils of the southwestern United States, in *Soils and Quaternary Geology of the Southwestern United States*, edited by D. L. Weide, *Spec. Pap. Geol. Soc. Am.*, *203*, 1–22.

Magistrale, H., and T. K. Rockwell (1996), The central and southern Elsinore fault zone, *Bull. Seismol. Soc. Am.*, *86*, 1793–1803.

Mann, P. (2007), Global catalogue, classification and tectonic origins of restraining and releasing bends on active and ancient strike-slip fault systems, in *Tectonics of Strike- Slip Restraining and Releasing Bends*, edited by W. D. Cunningham and P. Mann, *Geol. Soc. Spec. Publ.*, *290*, 13–142.

Matti, J. C., and D. M. Morton (1993), Paleogeographic evolution of the San Andreas fault in southern California: A reconstruction based on a new cross-fault correlation, in *The San Andreas Fault System: Displacement, Palinspastic Reconstruction, and Geologic Evolution*, edited by R. E. Powell, R. J. Weldon, and J. C. Matti, *Geol. Soc. Am. Mem.*, *178*, 107–159.

Matti, J. C., D. M. Morton, and B. F. Cox (1985), Distribution and geologic relations of fault systems in the vicinity of the central Transverse Ranges, southern California, *U.S. Geol. Surv. Open File Rep.*, *85-865*, 27 pp.

Matti, J. C., B. F. Cox, D. M. Morton, R. V. Sharp, and T. King (2002), Fault-bounded Neogene sedimentary deposits in the Santa Rosa Mountains, Southern California; crustal stretching or transpressional uplift?, *Geol. Soc. Am. Abstr. Programs*, *34*(6), 124.

Matti, J. C., D. M. Morton, B. F. Cox, G. P. Landis, V. E. Langenheim, W. R. Premo, R. Kistler, and J. R. Budahn (2006), Fault bounded late Neogene sedimentary deposits in the Santa Rosa Mountains, Southern CA: Constraints on the evolution of the San Jacinto fault, *Eos Trans. AGU*, *87*(52), Fall Meet. Suppl., Abstract T21B-0407.

Meade, B. J., and B. H. Hager (2005), Block models of crustal motion in southern California constrained by GPS measurements, *J. Geophys. Res.*, *110*, B03403, doi:10.1029/2004JB003209.

Meisling, R., and K. Weldon (1989), Late Cenozoic tectonics of the northwestern San Bernardino Mountains, southern California, *Geol. Soc. Am. Bull.*, *101*, 106–128, doi:10.1130/0016-7606(1989)101<0106:LCTOTN>2.3.CO;2.

Mencher, E., H. J. Fichter, J. M. Patterson, H. H. Renz, R. H. Robie, and W. E. Wallis (1953), Geology of Venezuela and its oil fields, *Am. Assoc. Petrol. Geol. Bull.*, *37*, 690–777.

Millman, D. E., and T. K. Rockwell (1986), Neotectonics of the Elsinore fault zone in Temescal Valley, California, in *Neotectonics and Faulting in Southern California*, edited by P. Ehlig, pp. 159–166, Geol. Soc. of Am., Boulder, Colo.

Morton, D. M., and J. C. Matti (1993), Extension and contraction within an evolving divergent strike-slip fault complex: The San Andreas and San Jacinto fault zones at their convergence in southern California, in *The San Andreas Fault System: Displacement, Palinspastic Reconstruction, and Geologic Evolution*, edited by R. E. Powell, R. J. Weldon, and J. C. Matti, *Geol. Soc. Am. Mem.*, *178*, 217–230.

Morton, D. M., and F. C. Miller (1987), K/Ar apparent ages of plutonic rocks from the northern part of the Peninsular Ranges batholith, southern California, *Geol. Soc. Am. Abstr. Programs*, *19*, 435.

Mueller, K. J., and T. K. Rockwell (1995), Late Quaternary activity of the Laguna Salada Fault in northern Baja California, Mexico, *Geol. Soc. Am. Bull.*, *107*, 8–18, doi:10.1130/0016-7606(1995)107<0008:LQAOTL>2.3.CO;2.

Opdyke, N. D., E. H. Lindsay, N. M. Johnson, and T. Downs (1977), The paleomagnetism and magnetic polarity stratigraphy of the mammalbearing section of Anza Borrego State Park, California, *Quat. Res.*, *7*, 316–329, doi:10.1016/0033-5894(77)90024-2.

Pinault, C. T. (1984), Structure, tectonic geomorphology and neotectonics of the Elsinore fault zone between Banner Canyon and the Coyote Mountains, Southern California, MS thesis, 231 pp., San Diego State Univ., San Diego, Calif.

Pinault, C. T., and T. K. Rockwell (1984), Rates and sense of Holocene faulting on the southern Elsinore fault: Further constraints on the distribution of dextral shear between the Pacific and north American plates, *Geol. Soc. Am. Abstr. Programs*, *16*, 624.

Rockwell, T., C. Loughman, and P. Merifield (1990), Late Quaternary rate of slip along the San Jacinto fault zone near Anza, Southern California, *J. Geophys. Res.*, *95*, 8593–8605, doi:10.1029/JB095iB06p08593.

Rockwell, T., M. Bergmann, and M. Kenney (2000), Holocene slip rate of the Elsinore fault in Temecula Valley, Riverside County, California, in *Geology and Enology of the Temecula Valley*, edited by B. Birnbaum and K. Cato, pp. 105–118, San Diego Assoc. of Geol., San Diego, Calif.

Shirvell, C. R., D. F. Stockli, G. J. Axen, and M. Grove (2009), Miocene-Pliocene exhumation along the west Salton detachment fault, southern California, from (U-Th)/He thermochronometry of apatite and zircon, *Tectonics*, *28*, TC2006, doi:10.1029/2007TC002172.

Spelz, R. M., J. M. Fletcher, L. A. Owen, and M. W. Caffee (2008), Quaternary alluvial-fan development, climate and morphologic dating of fault scarps in Laguna Salada, Baja California, Mexico, *Geomorphology*, *102*, 578–594, doi:10.1016/j.geomorph.2008.06.001.

Spotila, J. A., and K. Sieh (2000), Architecture of transpressional thrust faulting in the San Bernardino Mountains, southern California, from deformation of a deeply weathered surface, *Tectonics*, *19*, 589–615, doi:10.1029/1999TC001150.

Spotila, J. A., K. A. Farley, and K. Sieh (1998), Uplift and erosion of the San Bernardino Mountains, associated with transpression along the San Andreas fault, CA, as constrained by radiogenic helium thermochronometry, *Tectonics*, *17*, 360–378, doi:10.1029/98TC00378.

Spotila, J. A., M. A. House, A. E. Blythe, N. Niemi, and G. C. Bank (2002), Controls on the erosion and geomorphic evolution of the San Bernardino and San Gabriel Mountains, southern California, in *Contributions to Crustal Evolution of the Southwestern United States*, edited by A. Barth, *Spec. Pap. Geol. Soc. Am.*, *365*, 205–230, doi:10.1130/0-8137-2365-5.205.

Steely, A. N., S. U. Janecke, R. J. Dorsey, and G. J. Axen (2009), Early Pleistocene initiation of the San Felipe fault zone, SW Salton Trough, during reorganization of the San Andreas fault system, *Geol. Soc. Am. Bull.*, *121*, 663–687, doi:10.1130/B26239.1.

Stirling, M. W., S. G. Wesnousky, and K. Shimazaki (1996), Fault trace complexity, cumulative slip, and the shape of the magnitude-frequency distribution for strike-slip faults: A global survey, *Geophys. J. Int.*, *124*, 833–868, doi:10.1111/j.1365-246X.1996.tb05641.x.

Swanson, M. T. (1989), Sidewall ripouts in strike-slip faults, *J. Struct. Geol.*, *11*, 933–948, doi:10.1016/0191-8141(89)90045-X.

Swanson, M. T. (2005), Geometry and kinematics of adhesive wear in brittle strike-slip fault zones, *J. Struct. Geol.*, *27*, 871–887, doi:10.1016/j.jsg.2004.11.009.

Todd, V. R. (2004), Preliminary geologic map of the El Cajon 30′ × 60′ Quadrangle, southern California, version 1.0, *U. S. Geol. Surv. Open File Rep.*, *2004-1361*, 30 pp.

Todd, V. R., S. E. Shaw, and J. M. Hammarstrom (2003), Cretaceous plutons of the Peninsular Ranges Batholith, San Diego and westernmost Imperial Counties, California: Intrusion across a Late Jurassic continental margin, in *Tectonic Evolution of Northwestern Mexico and the Southwestern USA*, edited by S. E. Johnson et al., *Spec. Pap. Geol. Soc. Am.*, *374*, 185–235.

Vaughan, P., and T. Rockwell (1986), Alluvial stratigraphy and neotectonics of the Elsinore fault zone at Agua Tibia Mountain, Southern California, in *Neotectonics and Faulting in Southern California*, edited by P. Ehlig, pp. 177–191, Geol. Soc. of Am., Boulder, Colo.

Wakabayashi, J., J. V. Hengesh, and T. L. Sawyer (2004), Four-dimensional transform fault processes: Progressive evolution of stepovers and bends, *Tectonophysics*, *392*, 279–301, doi:10.1016/j.tecto.2004.04.013.

Weber, F. H. (1977), Seismic hazards related to geologic factors, Elsinore and Chino fault zones, northwestern Riverside county, California, *Calif. Div. Mines Geol. Open File Rep.*, *77-4*, 96 pp.

Weldon, R. J., II, K. M. Scharer, T. E. Fumal, and G. P. Biasi (2004), Wrightwood and the earthquake cycle: What a long recurrence record tells us about how faults work, *GSA Today*, *14*, 4–10, doi:10.1130/1052-5173(2004)014<4:WATECW>2.0.CO;2.

Wesnousky, S. (1988), Seismological and structural evolution of strike-slip faults, *Nature*, *335*, 340–343, doi:10.1038/335340a0.

Wesnousky, S. (1990), Seismicity as a function of cumulative geologic offsets: Some observations from southern California, *Bull. Seismol. Soc. Am.*, *80*, 1374–1381.

Winker, C. D. (1987), Neogene stratigraphy of the Fish Creek-Vallecito section, southern California: Implications for early history of the northern Gulf of California and the Colorado Delta, PhD thesis, 494 pp., Univ. of Ariz., Tucson.

Winker, C. D., and S. M. Kidwell (1996), Stratigraphy of a marine rift basin: Neogene of the western Salton Trough, California, in *Field Conference Guidebook and Volume for the American Association of Petroleum Geologists*, edited by P. L. Abbott and J. D. Cooper, pp. 295–336, Pacif. Sec. Am. Assoc. Petrol. Geol, Bakersfield, Calif.

Woodard, G. D. (1963), The Cenozoic succession of the West Colorado Desert, San Diego and Imperial Counties, southern California, PhD thesis, 173 pp., Univ. of Calif., Berkeley.

Yule, D., and K. Sieh (2003), Complexities of the San Andreas fault near San Gorgonio Pass: Implications for large earthquakes, *J. Geophys. Res.*, *108*(B11), 2548, doi:10.1029/2001JB000451.

G. J. Axen, Department of Earth and Environmental Science, New Mexico Institute of Mining and Technology, 801 Leroy Pl., Socorro, NM 87801, USA.

R. J. Dorsey and T. C. Peryam, Department of Geological Sciences, University of Oregon, Eugene, OR 97403, USA. (rdorsey@uoregon.edu)

M. E. Kairouz, AMEC Environment and Infrastructure, 115 W. Abeyta St., Suite A, Socorro, NM 87801, USA.